TU WIEN TECHNISCHE UNIVERSITÄT WIEN Vienna | Austria

SEMPERIT Ⓢ

Diplomarbeit

Investigations on the influence of surface structure and modification on ozone resistance of elastomers

durchgeführt von

Matthias Schöbinger, BSc

bei der Semperit Technische Produkte Gesellschaft m.b.H.
und am Institut für Angewandte Synthesechemie der TU Wien, E163
unter der Leitung von

Dr. Roman Hochenauer und Dr. Armin Holzner (Semperit)
Prof. Dr. Peter Gärtner (TU Wien)

It is a noble ambition to endeavor to fill the short span of our lives with deeds of lasting value. To a truly noble nature, there is no thought less endurable, yea, more repulsive, than to vanish utterly from the scene of life leaving no trace of useful accomplishment, to depart from this world without having contributed to the capital of the higher assets of humanity, to be physically alive and mentally dead, and to be forgotten by his contemporaries as soon as his eyes are closed.[1]

Christian Friedrich Schönbein.

Danksagung

Table of contents

1 Zusammenfassung

Die negativen Auswirkungen von Ozon auf Gummi nehmen eine wesentliche Stellung in der Zersetzung von Gummiprodukten ein und wirken daher limitierend auf die Lebensdauer von Elastomermaterialien, welche vielfältigst angewendet werden. Dieser Ozonangriff findet hauptsächlich an C-C-Doppelbindungen der Polymerhauptkette statt und führt zu charakteristischen Ozonrissen, jedoch nur, wenn sich das Material während des Angriffs in einem gedehnten Zustand befindet.

Die Gummiindustrie wendet zwei Hauptstrategien an, um das Risiko eines verfrühten Materialversagens durch Ozonalterung zu verhindern: Erstens werden gesättigte Polymere wie EPDM eingesetzt, um die fatale Ozonisierungsreaktion der C-C-Doppelbindungen zu verlangsamen. Zweitens werden chemische Additive wie paraffinische Wachse oder Antiozonanten eingesetzt, um die Ozonierung des Materials aktiv zu verhindern. Da die Verwendung von gesättigten Polymeren auf gewisse Anwendungsfelder limitiert ist, ist die zweite Herangehensweise die universellere und billigere Methode.

Da der Zersetzungsprozess durch höhere Ozonhintergrundkonzentrationen beschleunigt wird, führt die aufgrund des Klimawandels stetig ansteigende Ozonmenge in der Troposphäre zu einer verkürzten Lebensdauer von Elastomeren. Zusätzlich sind nicht alle Gummianwendungen mit Antiozonanten kompatibel und weiters könnten manche dieser Antiozonanten in naher Zukunft aufgrund ihrer Reproduktionstoxizität verboten werden.

Frühere Beobachtungen von Semperit zeigen alternative Mechanismen, welche möglicherweise die Ozonstabilität von Gummi beeinflussen könnten: Erstens könnte eine Oberflächenvorpassivierung mit Ozon an ungestrecktem Gummi zu einer positiven Beeinflussung der Ozonstabilität führen. Zweitens wurde eine Abweichung zwischen der Ozonstabilität von Hydraulikschlauchdecken und Laborprüfkörpern entdeckt, welche aus demselben Material gefertigt worden waren. Diese Divergenz kann einem oder mehreren abweichenden Produktionsparametern zugeordnet werden.

In dieser Arbeit wurden beide zuvor beschriebenen Phänomene untersucht. Weiters wurden chemische Oberflächenmodifikationen mit einem möglicherweise positiven Einfluss auf die Ozonstabilität von Gummiprodukten entwickelt und getestet.

Mit Hilfe einer DOE-Methodik (Design of Experiments) konnten statistisch signifikante Produktionsparameter, welche die Ozonstabilität beeinflussen, identifiziert werden. Dreidimensionale Oberflächenstrukturen und ein großes Oberflächen-zu-Bulk-Verhältnis kristallisierten sich als signifikant negative Einflüsse heraus.

Überdies zeigte sich, dass die Reaktion der C-C-Doppelbindungen, welche an der Oberfläche des ungedehnten Gummis liegen, mit Ozon keine weiteren Ozonangriffe auf den gedehnten Gummi verhindern.

Etliche chemische Oberflächenmodifikationen wurden ausgearbeitet und auf ihre Auswirkung auf die Ozonstabilität von Elastomeren getestet. Diese Reaktionen wurden mit Hilfe von ATR/FT-IR-, XPS- und SFE-Messungen charakterisiert. Chlorierungsreaktionen mit kurzer Reaktionszeit zeigten eine Verlängerung der rissfreien Zeit um das 3- bis 9-fache im Vergleich zum Blank. Epoxidierungsreaktionen mit m-CPBA verbesserten die zuvor genannte Zeit sogar um einen Faktor 25 und höher.

2 Abstract

The adverse effects of ozone on elastomers depicts a crucial part in the degradation of rubber products and therefore sometimes limits the durability of rubber parts used in manifold applications. This attack proceeds mainly on C-C-double bonds of the polymeric main chain, resulting in characteristic ozone cracks, if strain is applied on the rubber material during the attack.

The rubber industry applies two main strategies in order to reduce the risk of a premature failure in application due to ozone attack: Primarily, saturated polymers – like EPDM – are deployed in order to slow down the severe ozonolysis reaction of C-C-double bonds. On the other hand, chemical additives like paraffinic waxes or antiozonants are used to actively prevent the ozonation of the material. However, as the usage of saturated polymers is limited to certain fields of application, the second approach may be still the more universal and also less expensive one.

Since the degradation process is accelerated if higher ground-level background ozone concentrations prevail, the steady rise of the ozone amount in the atmosphere – due to climate change – results in a shortened lifespan of rubber goods. In addition, not all applications are compatible with antiozonants and the usage of some of them may face restrictions – because of their toxicity – in the near future.

Earlier observations at Semperit may suggest alternative mechanisms to influence the ozone resistance of rubber: Firstly, a surface pre-passivation with ozone at unstrained condition, which may affect the ozone resistance in a positive way, was discovered. Secondly, Semperit found a divergence in the ozone resistance of hydraulic hose covers and laboratory test specimens, that were made of the same elastomeric material. This divergence can be attributed to one or more differing production parameters.

In this thesis both phenomena were investigated and moreover chemical surface modifications with a positive impact on the ozone resistance of rubber products were developed and tested.

With the help of a DOE (Design of Experiments) approach, statistically significant production parameters influencing the ozone stability could be identified. Three-dimensional surface structures and a high surface to bulk ratio emerged as significant adverse parameters.

Furthermore, it turned out that the reaction of C-C-double bonds – located at the unstretched rubber surface – with ozone, does not prevent a further attack of ozone on the strained rubber material.

Several chemical surface modifications were elaborated and tested on their effect on the ozone resistance of elastomers. These reactions were characterized with ATR/FT-IR, XPS and SFE measurements. Chlorination reactions with short reaction times showed an enhancement of the crack free period with a factor of 3-9, compared to the unmodified blank. Epoxidation reactions with m-CPBA improved this factor even to 25 and higher values.

3 Introduction

3.1 Elastomers

3.1.1 Synopsis

Elastomers (also referred to as rubber) are commonly used, as an engineering material, which finds its application, due to its unique physical properties, in a wide range of products.

Raw rubber, the starting material in the production of elastomers, consists of cross-linkable polymers and various further components as illustrated in Table 1. When raw rubber is heated or deformed it exhibits viscous flow, enabling molding processes like extrusion or injection molding. In contrast to cured rubber, raw rubber is soluble in some organic liquids like toluene or benzene.[2]

In order to obtain the cured product from its precursor, the polymer chains need to be partially crosslinked. This heat treatment process, called vulcanization or curing, is also defined as an act of addition, re-establishment or improvement of elastic properties to the material. The cross-links nature can be covalent or of a weak interaction.[2]

The unique elastic properties are based on a completely different energy storage mechanism of elastomers (entropic elasticity) in comparison to other materials (energetic elasticity), like metals or thermoplastics. In the case of heat absorption normally internal energy adaptions proceed. In order to do so metals change their interatomic distances and thermoplastic materials their bond angles, so as to amend to the new conditions. Therefore, both materials will cool when elongated. On the contrary elastomers show an evolution of heat when they get stretched. This is due to the fact that the elongation process forces the elastomer in a higher ordered state, decreasing its entropy. The before mentioned lowered entropy is responsible for the restoring forces – since the entropy increases again after the applied strain has vanished and the material returns to the initial position– leading to the earlier mentioned unique elastic properties of elastomers.[2]

Table 1: typical components of a rubber recipe

component	mass fraction in phr
polymer	100
softener/plasticizer	0-250
fillers	0-250
processing aids	0-10
anti-ageing agents	0-10
activators	1-10
cross-linking substances	1-5
accelerator	0-5

The aforementioned addition of different other components to the polymer have manifold reasons.

Softeners respectively plasticizers are usually added to improve the processibility via viscosity adjustment. Moreover, the softener enhances the distribution of the filler and influences the

vulcanizate properties like hardness, elasticity, stress-strain behavior and low temperature flexibility. Based on the aforementioned properties of the softener one can distinguish between processing oils, which mainly improve the processability, and extender oils, which mainly act as dilutants. The border between these categories blur easily. Components can only be used as softeners if: there is a chemical compatibility with the used polymer, they do not interact with the vulcanization system, they show little or no toxicity and they are not volatile at the vulcanization temperature. Mineral oils therefore depict one of the most used substance class as plasticizers.[3]

Fillers can be divided into two main categories, regarding their chemical properties and their interaction behavior in the rubber matrix.

Active fillers (e.g. medium/high active carbon black or silica) enhance the physical properties of the material (Figure 1) and therefore depict a crucial part in rubber materials. This activity depends on the filler's geometrical properties (particle size and structure) and chemical properties. The downside of the use of active fillers, is a possible worsening of the elastic properties of the material, as well as of the processing behavior due to an increase of compound viscosity.[3]
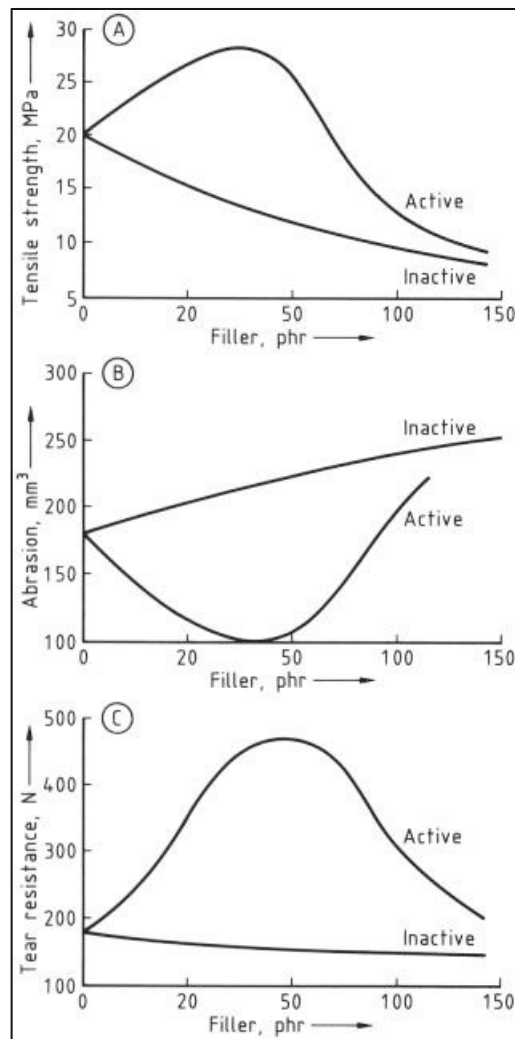

Figure 1: effect comparison of active and inactive fillers on natural rubber (A: tensile strength; B: abrasion; C: tear resistance)[3]

Inactive fillers on the other hand do not interact with the rubber matrix and therefore do not impart mechanical strength to the rubber. However, they may improve specific properties like compression set (e.g. low active carbon black), flame retardancy (e.g. aluminum hydroxide) or simply act as a cost reducing diluting material (e.g. chalk).

Processing aids are added to the engineering material in smaller amounts, compared to the already discussed components. They are used in order to enhance the processability of the rubber in a chemical or physical way. The specific problems that occur during rubber processing differ from case to case. The following tasks can be improved through the addition of the suitable processing aid:

- viscosity reduction
- polymer blending
- dispersion
- lubrication/flow improvement
- tack between rubber parts
- release process (demolding)

Anti-ageing agents are added to the rubber to protect it from external damages, excluded are damages due to mechanical influences like tearing or wearing. The earlier mentioned external damages can alter the bulk, due to oxidation, heat, hot liquids or rubber poisons, but also affect the surface (e.g. dynamic oxygen cracking, ozone cracking (*c.f.* 3.4), crazing or frosting). The material therefore suffers from: hardening, softening, cracking, loss of elasticity or toughness, or visual surface changes.[3]

The crosslinking process is based on sulfur or on sulfur-free cross-linking agents like peroxides. In the case of sulfur, the polymeric chains are crosslinked at their double bonds, thus as soon as the polymer exhibits saturation, a different cross-linking agent – typically on the base of a peroxide – needs to be used. Sulfur is applied either in its elemental form, where the solubility in the rubber matrix can be limited, or in form of organic compounds (e.g. TMTD (tetramethylthiuram disulfide), DTDM (dithiodimorpholine), 2-(morpholinodithio)benzothiazole, etc.). In order to accelerate the reaction time and decline the amount of sulfur, hence improving the ageing resistance of the rubber, accelerators (e.g. substances of the groups of sulfenamides, thiazoles, thiurams, etc.) are employed. To evolve the full activity of accelerators and therefore elevate the cross-linking density, activators (e.g. zinc oxide in combination with stearic acid) are added to the vulcanization system. Looking at peroxidic vulcanization agents (e.g. acyl peroxides, perketals, and alkyl or aralkyl peroxides), activators are not necessary, but due to interactions with other components of the rubber, different coagents might be added. The peroxidic compounds decompose into radicals at specific temperatures, abstract hydrogen atoms from the polymeric main chain and as a result initiate the cross-linking process.[3]

Since the properties of the polymer itself and the anti-ageing agents – more precisely the antiozonants – are crucial for this thesis, they are further discussed in chapter 3.1.2 (*cf.* 3.1.2) and chapter 3.5.1 (*cf.* 3.5.1).

3.1.2 Polymer types

Since the polymer is the main component of the elastomer, it is no wonder that its chemical properties are predominantly influencing the behavior of the whole material. Polymers can be roughly classified into different categories as can be seen in the subsequent table (Table 2).

Table 2: rough categorization of different polymers according to their chemistry

chemical properties of the polymer	properties of the rubber material
saturated main chain	weather, ozone and heat resistant
unsaturated main chain	low-temperature resistant, good mechanical properties
polar monomers	oil resistant
halogenated monomers	flame-retardant, improved weather resistance
silicone containing monomers	low-temperature, weather, heat, oil resistant, flame-retardant
flour containing monomers	chemical, weather, heat, oil resistant, flame-retardant

In the following the properties of a few different polymers – that were used predominantly in this thesis – are discussed. They depict only a small selection of the whole variety of polymers used in the rubber industry.

3.1.2.1 *Natural Rubber (NR)*[4]

Natural rubber is harvested from seed bearing plants, mainly *hevea brasiliensis*, as a dispersion of *cis*-1,4-polyisoprene in water. The process towards solid NR is not further discussed herein. Solid NR exhibits several advanced properties compared to various synthetic rubber: improved structural stability, elasticity, cold flexibility, dynamic properties and abrasion resistance. Moreover, NR shows a high building tack and green strength, as well as good extrusion and calendaring properties. Low oil- and ageing-resistance are the disadvantages of this material. Due to its special properties the biggest application area for solid NR are tires, especially truck tires, but also spring elements and buffers. When NR is strongly elongated, one has to be aware of its elongation crystallization properties. Nevertheless, the formed crystals persist even after the applied strain has vanished, thus resulting in a difference between loading and unloading curves. This crystallization leads to an anisotropy of the mechanical properties.
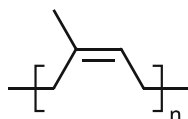
Scheme 3-1: cis-1,4-polyisoprene

3.1.2.2 Styrene Butadiene Rubber (SBR)[5, 6]

SBR is made of styrene and 1,3-butadiene by using a free radical emulsion process, yielding a pure random copolymer, or a solution process by anionic initiation, where also true block copolymers can be produced. The copolymerization in solution (e.g. in nonpolar hydrocarbons) can be initiated by butyllithium, leading mainly to a 1,4-configuration of the diene component. The random aligned SBR is used in standard rubber applications like tires, hoses and conveyor belts, as this material shows exceptional abrasion, water and crack growth resistance. Since E-SBR is higher branched and exhibits a wider molar mass distribution, it is more easily processed in comparison to S-SBR. Moreover, E-SBR has a higher tear and tensile strength but S-SBR exhibits higher modulus and green strength. The downsides of SBR are insufficient ozone, chemical and heat resistance.
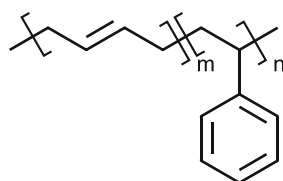
Scheme 3-2: SBR

3.1.2.3 Butadiene Rubber (BR)[5, 6]

Butadiene rubber consists mainly (92-98 %) of *cis*-1,4-polybutadiene and finds it application primary in the tire industry where it is used in tire treads, carcass stocks and sidewalls. Moreover, BR is used in conveyer belts, hoses and golf balls. The area of application is based on its high resilience, outstanding low-temperature properties and on the fact that BR is characterized by a low heat buildup during deformation, even at a high repetition rate. The processing properties of BR are tendentially not that ideal and strongly depend on its molar mass, molar mass distribution and its branching, and therefore on the polymerization parameters. BR is normally produced in solution and for the sake of stereoselectivity via a Ziegler-Natta system. Only in rare cases an emulsion process via a free radical route is chosen.
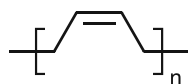
Scheme 3-3: cis-1,4-polybutadiene

3.1.2.4 Nitril Butadiene Rubber (NBR)[6]

NBR consists of 1,3-butadien and acrylonitrile as monomers. This polar rubber is easily processed and vulcanized with standard systems. The feature of the crosslinked rubber is its resistance to swelling in nonpolar liquids like oils, fats or fuels. Moreover, NBR is resistant to hot air and abrasion. The excellent swelling properties can be increased with the elevation of acrylonitrile content. Nonetheless, low temperature flexibility, elasticity, gas permeability, hardness and tensile strength are also properties that can be influenced by the used monomers

ratio. The aforementioned resistance to swelling in nonpolar liquids paths the way for this rubber to be employed in the automotive industry (e.g. brake linings), oil drilling industry and as oil resistant material in hydraulic and industrial hoses. Since NBR consists of an unsaturated main chain its ozone resistance properties are poor, however this can be boosted by blending with PVC, where homogeneity is a crucial parameter, or by selective hydrogenation. NBR is polymerized in an emulsion process, and since the acrylonitrile part is integrated into the polymer severely faster, a subsequent dosing has to be applied.
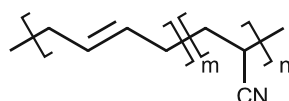
Scheme 3-4: NBR

3.1.2.5 Ethylene-Propylene-Diene Terpolymer (EPDM)[5]

EPDM belongs to the ethylene propylene elastomers and consists of a completely saturated main chain. The monomers are aligned randomly and since the diene component owns an unused double bond the vulcanization can not only be realized by peroxidic systems, but also by classical sulfur systems. As already depicted in table 2 (*c.f.* Table 2) the saturated backbone of EPDM is responsible for exceptional ozone, weather, heat, polar chemical and moisture resistance. Moreover, the material exhibits well insulating and low temperature properties. The properties of the polymer can be finely tuned by varying the following parameters: ethylene:propylene ratio, molar mass and its distribution, and the diene species and its amount. For this diene component subsequent substances are qualified: ethylidene norbornene, 1,4-hexadiene and dicyclopentadiene. However, ethylidene norbornene is normally used as it features good kinetic properties especially during the polymerization and during the vulcanization process. EPDM is mainly produced in a solution process; however, a suspension process is also feasible. The downside of EPDM rubber are its adhesion (tack) properties, nevertheless this issue can be fixed by blending with NR.
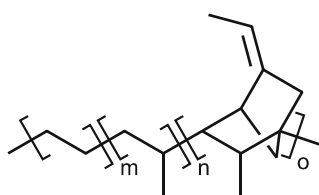
Scheme 3-5: structure of EPDM with ethylidene norbornene as diene component

3.2 Hydraulic hoses[7]

The main task of hydraulic hoses is the energy transfer, respectively the momentum transfer between the pressure generator and the working or control element. These hoses depict a flexible, but also a dimensionally stable connection and should feature a small pressure loss. They enclose the hydraulic fluid – usually mineral oils – which is the actual energy transfer

medium. The physical and chemical requirements of hydraulic hoses are internationally standardized.

To ensure all the needed properties the hydraulic hoses are constructed in a sandwich like structure, containing steel wires as reinforcement besides different rubber types. In Figure 2 a schematic buildup of a hydraulic hose is illustrated.
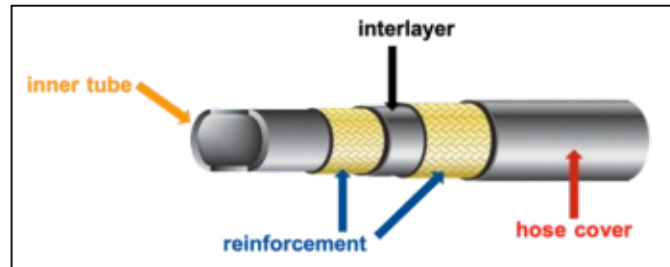
Figure 2: hydraulic hose buildup

3.2.1 Inner tube

The inner tube is in direct contact with the hydraulic medium and should therefore be stable, against commonly used hydraulic liquids. Since these liquids are typically based on mineral oils, the standard inner tube is made of oil resistance rubber (e.g. NBR). If a special hydraulic medium is used – for example chlorinated hydrocarbons or phosphate esters – fluorinated rubber may come into action. The inner tube should also be smooth and show a good temperature and pressure stability. Regarding its production, the inner tube is typically extruded on a mandrel (e.g. PP (polypropylene)), ensuring the correct inner diameter.

3.2.2 Reinforcement

The wire reinforcement can be applied in a braided or spiralized form on top of the pre-frozen inner tube, its function is clearly dedicated to ensure the hose's pressure stability. This stability is also characterized by the hose's volume consistency under pressure. Therefore, it is crucial to precisely maintain a defined and constant crossing angel between reinforcement layers, depicting a challenge for process engineers. Normally brass coated steel wires are used as reinforcement, only in special low pressure applications textile fibers come into action. If more than one reinforcement layer is used, interlayers of rubber are inserted to minimize possible internal abrasion and friction. Other than that, this interlayer acts as an adherent film.

3.2.3 Hose cover

The hose cover is functioning as a protecting mantle of the inner layers and should therefore be resistant to atmospheric influences like ozone, UV-light, high and low temperatures, etc. Furthermore, this layer should be abrasion proof, show a certain oil resistance and in special cases it should also feature a good flame retardancy. Depending on the designated use various types of rubber polymers may be used. This last layer is extruded on top of the inner layers. Before the finally assembled hose can be vulcanized in an oven, it gets wrapped into a nylon tape in order to secure the outside diameter and protect the hoses from sticking together.

3.3 Ozone

3.3.1 History

Ozone is a highly reactive molecule and was discovered as a distinct chemical substance in 1840 by Schönbein[i]. The newly discovered gaseous compound, which is an allotrope of oxygen (O_3, *c.f.* Scheme 3-8), was named by Schönbein after the Greek verb for smell: *ozein* (ὄζειν). Referring to the characteristic scent of ozone, which was known through the history of mankind accompanying lightning and in more recent history other electrical phenomena. Schönbein was also the first person who reported reactions with ozone: Studying the behavior of inorganic materials under ozone atmosphere, he mainly found the formation to oxides, peroxides and acids. In contrast organic materials were not fully oxidized to CO_2 and H_2O, rather leading mostly to aldehydes and carboxylic acids. Schönbein conducted experiments with ozone and ethylene, therefore performing the first ozonolysis reaction (*c.f.* 3.3.2.1). As the history in ozone research can be separated into three periods, this first one is named after its discoverer: *Schönbein period* (1840-1902). It mainly deals with the discovery, preparation and structure identification of ozone. Moreover first reactions were introduced, primarily without identification of the reaction products.[8][9]

The second period – the *Harries period* (1903-1948) – was initiated with the first paper from Harries regarding ozone chemistry, approx. 100 more should follow. He found his interest in ozone after he started dealing with rubber chemistry. Harries hoped, he would be able to characterize the structure of rubber with the help of the ozonolysis reaction. To do so, he needed deeper understanding of ozone and its reactions with common organic compounds – mainly alkenes. His first structural analysis was performed on allyl acetone (Scheme 3-6). Furthermore, Harries managed to differentiate between two main reaction-paths of ozone: The first one a two-step reaction between a C-C-double bond and ozone (reaction ratio: alken:ozone=1:1) – the before-mentioned ozonolysis reaction – with an ozonide (Scheme 3-7) as intermediate. An early mechanistic background, of this widely known reaction, was proposed by Staudinger. In the course of the second type of ozone reactions – for instance a reaction between ozone and an aldehyde – only one of the three oxygen atoms were found in the product. The remaining two O-atoms formed molecular oxygen (O_2). Moreover, during the *Harries period,* the structure of ozonides (Scheme 3-7) was described by Rieche.[8][10]

The last and still ongoing period is named after Rudolf Criegee (*Criegee period*, 1948 till now), who was able to clarify the mechanism of ozonolysis in 1953 (*c.f.* 3.3.2.1). Therefore, Criegee combined not only the ideas of Harries, Staudinger, Pummerer and Rieche with his own findings, but he also made use of all the existing physical organic technology.[8][10]

---

[i] Christian Friedrich Schönbein was born on October the 18th in 1799, as one of eight siblings. His family lived in Metzingen, Germany which is situated approx. 30 km south of Stuttgart. After his confirmation, Schönbein was sent to a chemical factory at Böblingen by his father – a dyer by profession – in order to financially support the family. In this factory he also received his first lectures in physics and chemistry. Schönbein studied French, Latin, mathematics, philosophy and chemistry, parallel to his job. In 1820 he was successfully examined by Professor Kielmeyer in Tübingen. After Schönbein worked as teacher and translator in Germany, France and Great Britain he obtained his doctorate in 1829 at the University of Basel. 1835 he received the full professorship for chemistry and physics at the aforementioned University. Schönbeins deep religiosity did not bar him from writing about 350 scientific publication. On August the 29th in 1868 the discoverer of ozone died in Baden.[1]
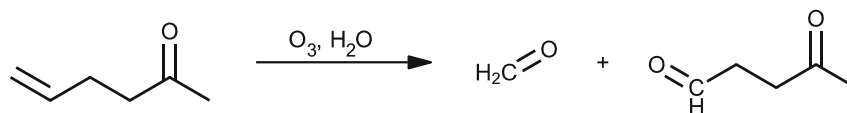
Scheme 3-6: structure analysis using ozone
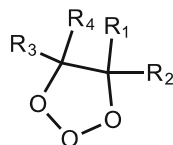
Scheme 3-7: ozonide

3.3.2 General reactivity and reactions with selected organic moieties

The chemical structure of ozone described either with a resonance (Scheme 3-8) or a diradical model, paths the way for ozone to undergo different reaction mechanisms. This versatility makes ozone a reaction partner to a great number of compounds originating from various different substance classes. Regarding the resonance model, all oxygen atoms are sp^2-hybridized, and each terminal oxygen atom forms a sigma bond with the middle O-atom. The left behind, non-binding sp^2-orbitals (two orbitals for each terminal and one for the middle atom) are filled each with one electron pair. The last four electrons are located in the π-molecular orbital which is formed with one p-atomic orbital of each oxygen atom. The diradical model in comparison, originating from *ab initio* calculations, suggests that ozone is in a diradical singlet ground state.[11]
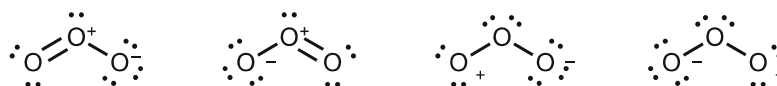
Scheme 3-8: the ozone molecule[11]

The resonance structures of ozone suggest therefore that it can react as a 1,3-dipole (e.g. *c.f.* 3.3.2.1), as an electrophile (e.g. *c.f.* 3.3.2.3 and 3.3.2.4) and as a nucleophile. Moreover, the second model enables diradical reactions (e.g. *c.f.* 3.3.2.2).

In Scheme 3-9 the reactivity of different organic moieties with ozone is shown. This variety facilitates selective reactions with different groups of one system, if the difference in reactivity is big enough.[12]
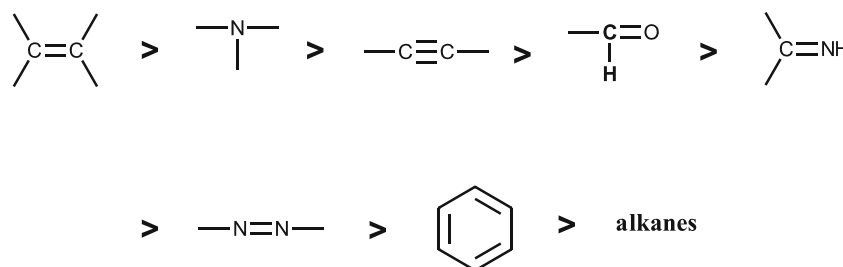
Scheme 3-9: ozone reaction rate comparison of different organic moieties[12]

3.3.2.1 Carbon double bonds

The ozone attack on C-C-double bonds ultimately leads to the cleavage of the carbon bond, therefore this reaction is called ozonolysis. After ozone reacts with the carbon double bond in a concerted one step 1,3-dipolar cycloaddition, an instable intermediate called molozonide is formed. This molozonide immediately decomposes to a carbonyl compound and a zwitterion (carbonyl oxide), which then react to the ozonide. Normally – due to its explosivity – the ozonide is not isolated, but rather converted into carbonylic compounds in consecutive steps.[13, 14]
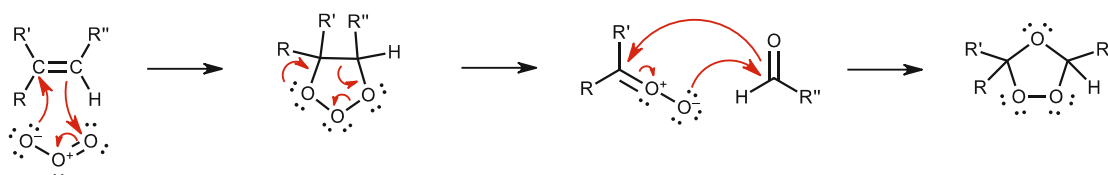
Scheme 3-10: ozone attack on C-C-double bond[14]

3.3.2.2 C-H-bonds

The ozonation of higher alkanes leads to the formation of alcohols, peroxides, esters, ketones and carboxylic acids. When decane is ozonated for instance, this reaction forms all possible ketones and alcohols with ten carbons and moreover ethanol, pentanol, hexanol and traces of other substances. Regarding the reactivity of different alkane carbon atoms, primary carbon atoms react slower than tertiary carbon atoms do.[15]

There are two possible mechanistic explanations for the reaction of carbon-hydrogen bonds with ozone. The first one depicts a radical mechanism initiating autooxidation. The other possibility is a more or less concerted 1,3-dipolar insertion. In the last case moieties possessing a +M-effect, bond to the attacked C-atom, stabilize the transition state and therefore accelerate the ozonation reaction.[15]
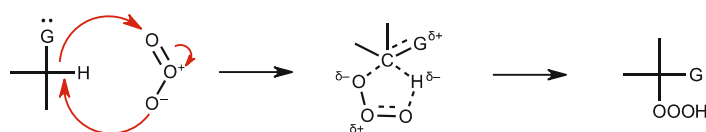
Scheme 3-11: 1,3-dipolare insertion[15]

3.3.2.3 Aromatic systems

Comparing the reactivity with ozone of an olefinic double bond, with a C-C-triple bond and with an aromatic system, a clearly order shows: C-C-double bond > C-C-triple bond > benzene bond. Therefore, it is not surprising that after the first ozone attack on an aromatic system was conducted successfully, the consecutive attacks are performed much easier – due to the loss of aromaticity. Ultimately the formation of peroxidic and non-peroxidic products in competing

reaction pathways are reported. Regarding a benzene molecule the reaction of three molecules ozone is feasible. When polymers, which contain an aromatic system (e.g. polystyrene), are ozonized, ring cleavage leads not only to carboxylic acids, but also to the formation of cross links.[16]

3.3.2.4 *Aromatic secondary amines*

Since amines in general exhibit a reactivity with ozone that is comparable to C-C-double bonds, it is strongly dependent on the individual substitution pattern of the amine, if higher reaction speeds can be reached. During the initial attack of ozone, the nitrogen atom of the amine depicts a nucleophile and the ozone acts as an electrophile. Further proceeding of the reaction can lead to either a side-chain oxidation – mostly by intramolecular proton abstraction (primary alkyl groups) or a 1,3-diopolar insertion (secondary alkyl groups) – or an amine oxide.

Especially looking at aromatic secondary amines, they form stable nitroxide radicals when reacting with ozone. Secondary phenylene diamines react prominently fast with ozone, making them useful for interesting applications (*c.f.* 3.5.1). Phenylene diamines are a perfect example how the substitutions pattern influences the ozonation reaction, in this special case a Wurster´s salt forms. p-Phenylene diamines (PPDA) form mesomeric stabilized cations in the Wurster's salt, explaining their high reactivity towards the salt. In comparison o-phenylene diamines react significantly slower with ozone, due to a sterically hindrance, that does not allow stabilization effects.[17]

3.3.3 Toxicity

Adverse effects of ozone on the human body were first mentioned in 1851 by Schönbein. He described chest pain, irritation of the mucous membranes and general breathing problems as symptoms after inhaling ozone. Small animals like rabbits or mice died even after minutes staying in ozone containing atmospheres. However, the precise mechanism behind the toxicity of ozone remained unknown at this point.[9]

After the ingestion of ozone – mainly through the lungs – the gaseous compound reacts completely with body tissue, due to its high reactivity. Yet it is this high reactivity that hinders O_3 to permeate into deeper tissue, leading to the following question: How can ozone initiate extrapulmonary effects like inflammatory reactions? An attempt to explain is given by subsequent line of thought. The airway lining consists of nearly 90 % lipids and therefore also of unsaturated fatty acids like oleic acid and palmitoleic acid. It comes to mind that these C-C-double bonds can easily be attacked by ozone, performing an ozonolysis reaction. As mentioned earlier (*cf. 3.3.2.1*) the Criegee mechanism suggests a formation of an ozonide and in the presence of water a conversation to aldehydes and hydroxy peroxides. It is believed that these lipid ozonation products (LOP) – as they are similar to already known lipid derived transducing molecules – can activate lipases and maybe other enzymes, initiating a whole signaling pathway (Figure 3). Gluthation, ascorbate and other antioxidants are the only defense against an attack of ozone on lipids, as they react in a competitional reactions. l-Palmitoyl-2-oleoyl-sn-glycerol-3-phosphocholine ozonide (POPC-Oz) is recognized and cleaved by

Phospholipase A_2 (PLA_2) in cell membranes leading among others to LOPs, this depicts another possible protective mechanism, at least for the membrane itself.[18]

Regarding the long-term effects of ozone on the human body, a study published in "The New England Journal of Medicine" analyzed data – originating from US metropolitan areas – of 448,850 subjects including 118,777 deaths through an 18-years follow-up period. By using a two-pollutant model ($PM_{2.5}$ and ozone) the two analyzed death risks – cardiovascular and respiratory risk – could be clearly attributed: Considering the risk of death from respiratory cause, a sharp increase was observed with an increase in ozone pollution. If one compares the risk of death from respiratory cause between the metropolitan area with the lowest ozone concentrations to the area with the highest concentration the risk of death is increased by three times.[19]
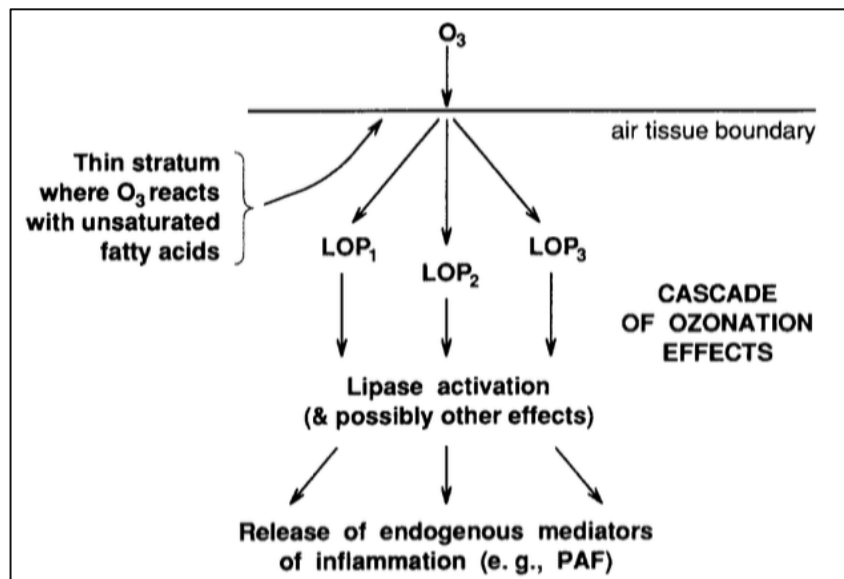
Figure 3: cascade mechanism: ozone toxicity[19]

3.3.4 Environment

In 1840 Schönbein was able to link the odor of ozone – which was only recently discovered by himself – to the odor occurring after an electrical storm. He then came up with the idea, that ozone can be found permanently in the atmosphere and Schönbein underpinned his idea successfully with measurements using iodine starch-paper.[9]

The surface ozone concentration in the Northern Hemisphere varies between 20-45 ppb, depending on the exact geographic location, elevation and anthropogenic influences. This fluctuation can be explained with the interplay of four main mechanisms: the formation, the transportation, the deposition and the distraction. The ozone background concentration is cycling through an annual maximum in spring, particularly in May. Nonetheless, the maximum's origin is not yet fully clarified, there are different attempted explanations: As the photochemical lifetime of anthropogenic ozone is elongated in winter, it is proposed that an accumulation of ozone could peak in spring. A different approach assumes that not ozone itself, but rather ozone precursors like anthropogenic emitted NO_X and hydrocarbons are accumulated

over winter. As the solar radiation is increased in spring these precursors convert over a photochemical pathway into ozone.[20]

Pre-industrial measurements – like Schönbein conducted in the 1840s – were not only semiquantitative, but also sensible for moisture and other oxidants, making a comparison to present measurements rather difficult. Even so, an anthropogenic influence on the surface ozone concentrations can not only be clearly seen as actual data is significantly elevated compared to pre-industrial data, but also due to high growth rates during the 70s and 80s. This global growth is based on the increasing emissions of ozone precursors, originating mainly from east Asia and distributed by intercontinental transport. Regarding the future trends IPCC combined 14 models in 2003 predicting a worldwide increase of the surface ozone concentrations during the 21st century. For most populated areas even the clean air standard of <80 ppb will be hardly achieved, affecting crops, vegetation and human health negatively. However, these models are limited due to omitting changes in the global climate.[20]

3.4 Ozone degradation of elastomers

In 1853 – during the *Schönbein period* (*cf.* 3.3.1) – Soret discovered the reaction of ozone with rubber. He reported a fast degradation of the rubber joints used in his ozone generator, mainly at low temperatures. The observed lower rate of the ozone attack at room temperature, could be attributed to the decreased ozone concentration, due to less ozone formation at elevated temperatures.[9]

This observed degradation phenomenon is mainly based on the ozonolysis reaction (*cf.* 3.3.2.1) of C-C surface double bonds, in special cases (e.g. natural rubber) the reaction advances into the bulk. Each surface double bond can be seen as an independent kinetic unit; hence the ozonolysis is following a bimolecular reaction. However, in saturated elastomers the reaction of ozone with C-H bonds (*c.f.* 3.3.2.2) can also result in a degradation of the material, although at a much slower rate.[21]

Yet, the chemical reaction between the elastomer and ozone alone do not lead to the characteristic ozone cracks (Figure 4). If strain is applied during the exposition of the material to ozone, the earlier mentioned carbonyl compound and the zwitterion, originating from the decomposed molozonide (*c.f.* 3.3.2.1), can leave the reaction cage and ultimately attack neighboring polymer chains and lead to their scission, instead of forming the ozonide. Furthermore, if the attacked macromolecules are aligned parallel to the direction of strain, the described process leads to microcracks. This applied strain must exceed a critical value (e.g. <10% for NR), which is distinctive of the material at a given ozone concentration and temperature. In the next step – assuming a constant ozone exposure and a constant applied stress – the prior formed microcracks will grow in depth and length. The number of cracks formed per area is depending on temperature and humidity, showing a directly proportional dependency. Although, with an increasing amount of cracks the depth and length decreases.[3,][22] The correlation between stress and the time between the start of ozone exposure, as well as the first observed crack is not that straight forward. It can be shown that with increased stress the first crack appears earlier, the crack free period goes through a minimum before advancing again.[23]

Additionally, during ozone exposure of rubber it is reported that the surface roughness increases with time. The ozone attack is also indicated by a stress relaxation of the material, even before cracks are visible.[23]

It has to be added that dynamic stress depicts a negative impact on the ozone resistance of rubber, due to the fact that unharmed polymeric chains bloom out of the bulk and therefore the surface is continuously renewed. This leads to more cleaved chains and consequently to an earlier material failure.[24]

At strained conditions, a degradation of non-resistant polymers (e.g. highly unsaturated polymers) starts with an ozone concentration as low as 1 ppb, depicting only a fraction of the average surface ozone concentration (*cf.* 3.3.4).[21] This low starting concentration demonstrates, that not only in critical areas (medical applications, aviation, space travel), where a material failure would be fatal or areas with increased ozone concentration (radiation areas, high voltage areas), need ozone protected elastomers, but also standard applications.[25]

Figure 4: cracks perpendicular to the direction of strain on an ozone exposed rubber specimen

3.5 Ozone protection of elastomers

3.5.1 State of the art strategies

The most obvious possibility to lower the risk of fatigue through ozone degradation is the usage of elastomers containing a very low number of C-C-double bonds, e.g., EPDM. However, EPDM is not only more expensive than other polymers, but its properties cannot fit all applications well, e.g., where polar elastomers are needed.[24]

It is these different applications that need appropriate solutions, currently there are two different chemical approaches that are in use. In the case of static applications, waxes are employed. Furthermore, the waxes can be subdivided into paraffinic- and microcrystalline waxes. In Table 3 their properties are compared.[24]

Table 3: properties of ozone protection waxes

property	paraffinic waxes	microcrystalline waxes
molecular weight in Da	350-420	490-800
crystallinity	highly crystalline	small, irregular crystals
melting range in °C	38-74	57-100
molecular properties	linear	branched

In order to protect the elastomer against ozone, the wax needs to build up a layer – which acts as a physical barrier – on the surface of the material. Therefore, the wax has to diffuse from the inside of the rubber to its outside, ideally in a controlled fashion to ensure a protective effect

for extended periods. This process is called blooming and is normally unwanted for other rubber components, thus the properties of the bulk would be altered.[24]

Since the solubility and diffusion rate is strongly depending on temperature, this parameter is the main influencing factor for the wax film thickness and therefore for the quality of the protection against ozone attacks. The level of the protection effect is directly proportional to the film thickness. Paraffin waxes hold their maximum film bloom by approx. 20 °C, in contrast microcrystalline waxes feature an operating optimum at 50-60 °C. In order to cover wider temperature ranges, different waxes can be mixed and used as a blend.[24]

Regarding dynamic applications antiozonants, which originate from the substance class of p-phenylene diamines (PPDAs, Scheme 3-12), are used. The ozone protection effect of PPDAs derives from its faster reaction with ozone compared to the reaction of rubber C-C-double bonds with ozone. For further information regarding the reaction mechanism see chapter 3.3.2.4 (*cf. 3.3.2.4*). If the different categories of PPDAs (Scheme 3-12) are compared in their rubber protecting effect, following order originates: alkyl-alkyl-PPDA>>alkyl-aryl-PPDA>>aryl-aryl-PPDA. In addition to the antiozonant activity PPDAs are also effective antifatigue agents. Since, the fatigue degradation follows a completely different mechanism (a mechano-oxidative mechanism) compared to the ozone attack, it is not surprising that the PPDAs are only the precursors of the later antifatigue agent, a nitroxyl radical species. This active species is a result of an earlier oxidation of the PPDA in-situ in the mechano-oxidized rubber. This nitroxyl radical terminates further occurring polymer radicals, preventing therefore fatigue cracks.[24]

PPDAs do not alter physical properties of the rubber in a significant way. If 6-PPD is compared to DPPD, it can be seen that 6-PPD is more effective than DPPD, but it migrates faster to the surface and is therefore not long lasting. The two compounds are often used combined to utilize both advantages.[24]

The downside of PPDAs is the staining –brownish, matt – of the materials surface and therefore antiozonants are incompatible with white rubber and colored rubber.

The addition of antiozonants also increases the diffusion of ozone waxes to the materials surface, without altering the composition of the formed surface film.[24]

Regarding the reproduction toxicity, 6-PPD is categorized under category 1B (presumed human reproductive toxicants). Moreover, for IPPD an up-to-date toxicity study is currently in their starting phase. Generally, it could be presumed that sooner or later all substances from the substance class of PPDAs will be classified in a similar matter and therefore will be limited or completely prohibited by ECHA. This emerging trend already has an effect on the PPDA market since IPPD production might slowly cease. In the long term it can be assumed that the range of PPDA-products will be more and more reduced until it will completely vanish.
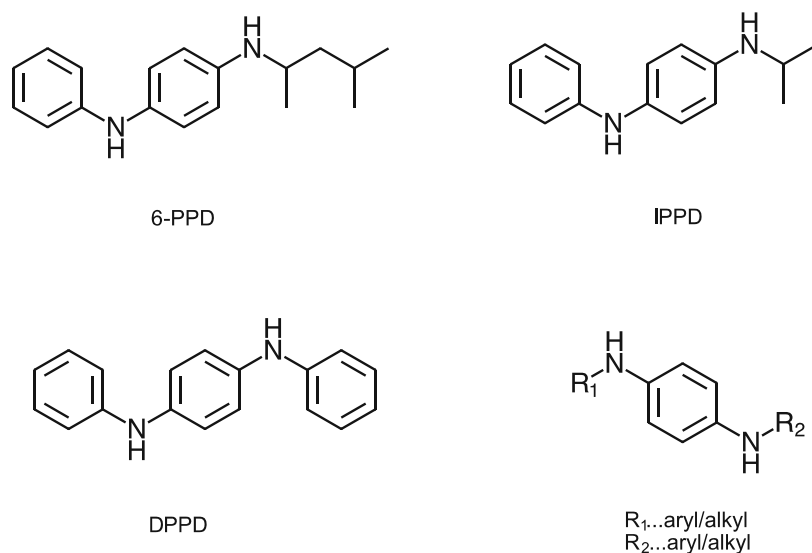
Scheme 3-12: common antiozonants and the general structure of PPDAs

3.5.2 Possible novel strategies

Regarding elastomers containing vulnerable surface C-C-double bonds, theoretically an efficient way to slow down or even prevent an ozone attack is illustrated by chemical surface modifications, decreasing the number of surface double bonds. There are plenty examples of elastomer surface modifications described in literature, seldom dealing with ozone protection.

3.5.2.1 Ozone pre-passivation

During investigations conducted earlier by Semperit, regarding market feedback about differences in the observed ozone durability of hydraulic hoses, the idea came up that pre-passivation with ozone – a chemical surface modification by ozone at un-stretched conditions – may decelerate further attacks of ozone under strain. This idea was underpinned by a short laboratory study, which will not be further described herein.

Early investigations made by Tucker suggest also a formation of such a protective passivation layer, as it is known from metals (oxide layer). This layer should be formed as long as the rubber is unstretched, otherwise the earlier mentioned ozone degradation starts.[26]

In Patent DE102008040209A1 – dealing with surface modifications of windshield wiper blades made of elastomers containing C-C-double bonds – an ozone pre-passivation is also proposed. It is stated that during the ozone treatment of unsaturated elastomers under no strain or strain remaining under a critical value, an ozonated surface layer builds up, preventing further ozonolysis and ozonolysis of the bulk. Since there is no or hardly any chain scission expected at low mechanical strain (*c.f.* 3.4.) Other than that, the formed layer may have more advantageous properties – like less friction and a higher wear resistance –especially regarding the use as a windshield wiper blade.[27]

3.5.2.2 Oxidation (UV/Cu/air)

During oxidation of rubber, scission and cross linking, two opposing mechanisms come into action. The reaction sequence starts with the formation of radicals as parts of the main chain cleave. These radicals may react in the further course with oxygen to peroxidic radicals, which ultimately can lead to new scissions. As can be imagined, the formed radicals can also lead to cross-linking through recombination processes. The diffusion of oxygen in the material is one parameter that affects the balance between scission and cross linking.[28]

Single bond scission is predominant, as the dissociation energy of single bonds is smaller compared to double bonds. This effect can be clearly seen, when rubber is analyzed in early oxidation stages, where no double bonds are lost.[28, 29]

Double bonds located in the main chain are attacked predominantly compared to side chains holding double bonds, this behavior opposes that of polymerization reactions where the side chain reacts preferentially.[29]

The herein described oxidation process can be accelerated by UV-light, elevated temperatures and metal impurities.[30]

However, the contrary observation that high concentrations of cobalt, manganese or copper ions can quench the earlier mentioned peroxidic radicals and therefore inhibit further oxidation processes, were also made. The quenching effectivity is based on the ability of the metal to undergo one electron transfer redox reactions.[31]

If one looks closely at the effects of copper salts on the rubber bulk, the adverse effects like lower crosslink density and decreased tensile strength, are manifest, but also strongly depending on the copper compound.[30] Often these adverse effects are attributed to its catalytic function, promoting rubber oxidation. However literature indicates also a disaggregation of the rubber leading to an increased surface area with double bond accumulation, facilitating in an accelerated oxidation.[32]

After the observation that an oxidized rubber surface is less susceptible to ozone attacks, copper salts, e.g. copper chloride, in combination with UV-light were used to build up such a protective layer. Since the copper was used only externally, no bulk oxidation were assumed.[33]

3.5.2.3 Dihydroxylation

Another possible way of surface functionalization is a dihydroxylation reaction with $KMnO_4$. It should be noted that the reaction mechanism of this reaction requires the presence of OH^- ions. Moreover, to avoid an attack of MnO_4^- at the earlier formed hydroxy moiety – leading to higher oxidation products like ketones or even chain scission – the aqueous solution should not be too basic. A pH-value of approx. 10 should be sufficient.[34-36]

3.5.2.4 Chlorination

The underlying mechanism of C-C-double bond halogenation reactions can proceed either ionic or radical.[37] This ionic mechanism is possible, because halogens – especially Cl_2 and Br_2 – are easy polarizable molecules. After the C-C-double bond induces a dipole, the halogen gets heterolytically cleaved. In the following the double bond and the halonium ion form a cyclic

intermediate. Since this intermediate is positively charged and strained, the reaction with the earlier formed halide anion proceeds very fast – forming the dihalogenide.[38]

The surface halogenation of elastomers is mainly used to adapt the surface energy or enhance the coefficient of friction (Scheme 3-14). More rarely this modification is described as a possibility to enhance ozone resistance of unsaturated elastomers. After fluorine, the second most used halogen is chlorine, often introduced through heated gas (Cl_2 (g)), solutions of Cl_2, in situ generated Cl_2 (e.g. acidified hypochlorite solution) or organic chlorination agents like trichloroisocyanuric acid (TCICA, Scheme 3-13).[39, 40]
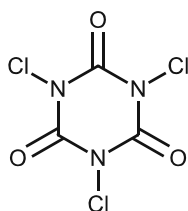
Scheme 3-13: trichloroisocyanuric acid (TCICA)

Another common application for chlorinated rubber is powder free gloves. Since the powder can lead to adverse health effects, chlorination of the materials (mostly NR) surface, is an appreciated replacement to lower the friction resistance. However, there are several downsides of this procedure e.g.: strong odor, possible skin irritations, over chlorination, poor reproducibility and the loss of needed physical properties.[41]
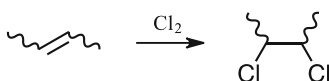
Scheme 3-14: schematic chlorination of a rubber C-C-double bond

3.5.2.5 Epoxidation

Epoxidation reactions depict an important part in organic chemistry. As a substituted alkene can be attacked from two sides, stereoselectivity plays a crucial role during epoxidation reactions. However, modern approaches mostly use transition metal complexes as catalysts, at this point especially the asymmetric epoxidation by Sharpless[42] should be mentioned. Nonetheless, racemic epoxidations still play a major role in laboratory and industrial synthesis. A widely known example is the chlorohydrin[43] process were *in-situ* produced hypochlorite is used as an oxidation agent.[44]

A simple direct epoxidation with sodium hypochlorite at a pH-value of about 10 can lead to the desired product. In order to boost the obtained yield, an *in-situ* generation of hypobromite can be utilized, since this species is more reactive. This *in-situ* generation can be achieved by the addition of potassium bromide in equivalent or catalytic dosage to the aqueous sodium hypochlorite solution.[44]

Another group of oxidizing agents are substances containing a peroxide moiety. Especially. m-CPBA – an aromatic peroxyacid (Scheme 3-15) – is often used. In comparison to other peroxides it is safely handled and the up-stream purification is more straightforward. US patent

5,310,819 proposes a surface epoxidation of unsaturated elastomers (Scheme 3-16) with peroxides (e.g. m-CPBA), in order to prolong oil resistance of cured rubber.[45]
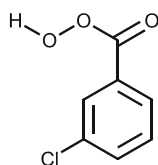
Scheme 3-15: m-CPBA...meta-chloroperoxybenzoic acid

Scheme 3-16: schematic epoxidation of a rubber C-C-double bond

3.5.2.6   Production parameters

During routine analysis, regarding the ozone resistance of elastomeric hydraulic hoses, Semperit found a divergence between laboratory test specimen (in accordance with ISO 1431-1:2012) and the hoses produced on industrial scale. The laboratory test specimen showed a significant elongated durability against ozone compared to the hoses. This divergence can be attributed to one or more parameters, which distinguish the production process of the hoses and the laboratory specimen.

3.6   Surface characterization

Since surface degradation processes, chemical surface modifications and surface coatings depict a crucial role in rubber chemistry, the characterization of those surfaces and moreover the evaluation of the underlaying mechanisms of earlier mentioned surface alterations is an essential tool in order to optimize elastomeric materials.[46]

Hereinafter a short overview of the three most common analytic technics should be given.

3.6.1   Attenuated Total Reflection – Fourier Transform Infrared Spectroscopy (ATR/FT-IR)

Since common elastomeric materials are thicker than the ideal transmission length (of about 20 µm), for the application of a transmission FT-IR experiment, attenuated total reflection is applied. The evanescent wave is penetrating the material and therefore gathering information in a depth of 0.5 to 2.0 µm. This penetration depth is dependent on the wavelength of the radiation, on the refractive indices of the sample and the ATR-element, and on the incidence angle. ZnSe and diamond are commonly used refractive elements, they mainly differ on their hardness. If a smaller penetration depth is needed, e.g. for the analyzation of thin films or black materials, Germanium is used as a refractive element. Additionally, advantages of the ATR

method are the absence of sample preparation and the fact that it is a nondestructive method.[47, 48]
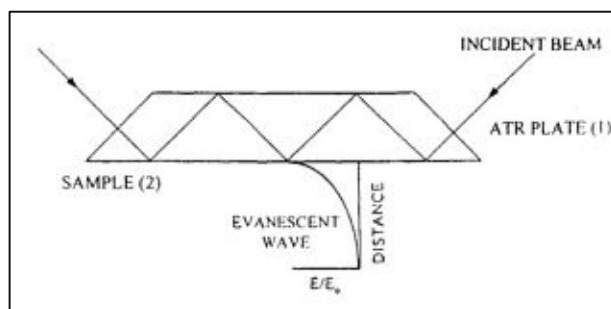
Figure 5: Total reflection in ATR-element[49]

3.6.2 Contact Angle (CA) and Surface Free Energy (SFE)

The CA measurement is a rather simple and cheap method, but should not be underrated, especially when combined with other analyzing techniques. A common method for the determination of the CA is the sessile drop method: After a certain amount of liquid is deposited on the specimen's surface, a defined angle between the surface and the liquid builds up. This is due to the balance of interfacial tensions between the solid, the liquid and the vapor. The correlation is described by the Young's equation (Equation 1) and only for ideal planar surfaces valid. Considering rough surfaces other theories have to be used e.g. the Wenzel model.[46]

After the determination of the CA of more than one suitable liquid (depending on the material) with known surface tension, the SFE can be computed. Therefore, different models are available. Today commonly used models include an error analysis, facilitating the interpretation of its outcomes. One main factor that differentiate between the SFE calculation theories is the consideration of different interactions between the liquid and the solid surface. For instance, the Owens/Wendt and the Fowkes theory, both a two-component model consider the disperse and the polar component. In contrast the van Oss theory further splits up the polar part into an acid and a base part making this model a three-component model.[50]

It has to be added that the term of "surface energy" is not universally defined in scientific literature and therefore strongly depended on the used model. Additionally, especially interfacial interactions between the liquid phase and polymeric materials are not yet fully understood.[50, 51]

Equation 1: Young's equation; γ...interfacial tension in N/m, L...liquid, V...vapor, s...solid phase, γ^0...equilibrium state[52]

$$\gamma_{LV}\cos(\theta) = \gamma_{SV}^0 - \gamma_{SL}$$

3.6.3 X-ray Photoelectron Spectroscopy (XPS)

Regarding the detailed analyzation of the outermost nanometer thick layers of the material, the XPS represents an outstanding analytical method. This method is capable of determining changes in the binding energy and therefore detects the chemical environment of nearly all

elements. With the help of XPS, the variation of the amount of existing- and the introduction of new functional groups, due to surface modifications, can easily be monitored. If different moieties with comparable binding energies are in the focus, information can be restricted due to resolution limitations. In this case the use of complementary surface characterization methods (e.g. SFE or ATR-FTIR, *c.f.* 3.6.1, 3.6.2) have to be consulted.[46]

The XPS is based on the photoelectric effect (Equation 2), so in order to gather information from the material it is irradiated with X-rays. The afterwards emitted photoelectrons are analyzed with an electron analyzer according to their intensity and energy. Since the interaction of the photoelectrons with external particles is unwanted, the device has to be operated at ultrahigh vacuum (UHV). The downsides of XPS measurements are that it is semi-quantitative, and a degradation of the sample is possible over time, due to damages initiated by X-rays. Moreover, surface contaminations of the specimens can become a problem.[46, 53]

In addition to the simple surface characterization, a depth profiling – with the help of Ar-sputtering – can be performed.[46]

For further insights see[53].

Equation 2: photoelectron effect; h...Planck constant in Js ,ν...photon frequency in Hz, E_B...binding Energy in J, E_K...kinetic energy in J, φ_a...spectrometer work function in J[53]

$$h\nu = E_B + E_K + \varphi_a$$

4 Scope

As depicted in chapter 3.3.4 (*cf.* 3.3.4) a steady rise in the tropospheric ozone background concentration, over the 21st century, will result in a significant shorter lifetime (*cf.* 3.4) of elastomeric products. Especially, products containing a high number of C-C-double bonds will be affected. Moreover, the downsides of the widely used antiozonants – regarding their incompatibility with white and colored rubber and the possible restrictions of this substance class, due to their reproduction toxicity (*cf.* 3.5.1) – are severe. Hence with regard to long lasting and therefore sustainable rubber products novel ozone protection strategies are highly needed. These strategies should not only be cheap, effective and environmentally friendly, but the procedures should also alter the materials bulk, and therefore its finely tuned properties, as little as possible.

Since two interesting observations that were made by Semperit – mentioned in chapter 3.5.2.1 (*cf. 3.5.2.1*) and chapter 3.5.2.6 (*cf. 3.5.2.6*) –exhibit mechanisms that may enhance the ozone resistance of elastomers, this thesis should investigate both phenomena, precisely. In addition, other promising chemical surface modifications (*cf.* 3.5.2), showing the potential to fulfill aforementioned demands, should be developed and evaluated.

5 Results and discussion

5.1 Production parameters

5.1.1 Identification of possible adverse parameters

In order to distinguish which production parameter is accountable for the earlier mentioned divergence (c.f. 3.5.2.6) in the ozone resistance, between laboratory test specimens acc. to ISO 1431-1:2012 and the cover of hydraulic hoses – produced in industrial scale – in a first step, the distinctive materials were compared for differences: Since the laboratory test specimens are produced in order to evaluate the ozone resistance (static or/and dynamic strain test) of the rubber product, the hoses and the specimen are made out of the same rubber formulation. Due to time saving issues the lab specimens are vulcanized at a higher temperature and shorter time, in comparison to the hoses (Table 4). The norm suggests a thickness of 2 mm for the test specimens; however, the hose's cover exhibits nearly half of that thickness. Another difference, between the two rubber products, is the inhomogeneous surface structure of the hoses. The application of the nylon tape, during the production is accounted for this imprint. In comparison, the test specimens exhibit a completely smooth surface. This left behind imprint can further vary due to the application of different tapes, as varying dimensions of the hoses require different tape widths. It was speculated, that these different tapes may feature different structures and therefore the left behind imprint may differ in roughness. Moreover, the tapes are reused for several production cycles and therefore different hose batches are produced with tapes of different age. Due to the fact that the tapes are applied with an overlap of 50 %, there is a prominent deepening crossing the hoses all around (*c.f.* Figure 20).

Table 4: production parameter differences between hydraulic hoses and static strain test specimen

production parameter	hydraulic hose	static strain test specimen
vulcanization	137 °C for 120 min	150°C for 60 min
thickness	hose cover approx. 0.8 mm	2.0 mm
nylon tape imprint	yes	no
different tapes	width depending on batch and hose dimension	-
tape age	varying from batch to batch	-
tape overlap	surface inhomogeneity	-

In order to evaluate a possible roughness difference between several tapes, the tapes were subjected to the microscopic analyzation of their roughness. Table 5 shows the results of these analyses and it can be clearly seen that the 70 mm width tape exhibits a ~20 % higher roughness compared to the 80 mm width tape. The 80 mm width tape with approx. 20 production cycles shows the smallest arithmetical mean height. This might be attributed to the strain that is applied, during the tape application in the production, flattening the nylon mesh.

Table 5: tape roughness comparison; mean from three measurements at different locations

parameter	70 mm tape	80 mm tape	80 mm tape 20 cycles
Sa (arithmetical mean height)	38.7 ± 0.8	32.1 ± 2.3	26.4 ± 4.3
Sz (maximum height)	401.2 ± 10.7	339.4 ± 48.9	301.4 ± 84.6
Sq (root mean square height)	48.0 ± 1.0	39.5 ± 3.2	33.0 ± 5.5
Sp (maximum peak height)	191.9 ± 20.8	175.1 ± 19.0	183.7 ± 56.7
Sv (maximum pit height)	209.3 ± 10.2	164.3 ± 30.5	117.7 ± 55.5

5.1.2 DOE-setup

After the differing parameters between production of the cover of hydraulic hoses and the lab specimen were defined, it was decided to recreate the mentioned parameters in the laboratory on rubber sheets. In order to evaluate which parameters have significant influence on the ozone resistance – but simultaneously save time and costs – a DOE was set up with the help of the software JMP and the in chapter 5.1.1 (c.f. 5.1.1) depicted factors. All possible primary and secondary interactions were considered, which are listed on the left side ("Term") in the Pareto diagram (Figure 8). Table 6 shows the 30 different combinations of production factors calculated by JMP, that were necessary for a statistically significant experiment.

Table 6: rubber sheets suggested by the DOE plan

rubber sheet	factors			
	thickness in mm	vulcanization temperature and time in °C / min	tape width in mm and tape age	overlap
MSS1P1	2	137/120	80 new	no
MSS1P2	0.8	137/120	80 old	yes
MSS1P3	2	137/120	80 old	no
MSS1P4	0.8	150/60	70 new	yes
MSS1P5	0.8	150/60	70 new	no
MSS1P6	0.8	137/120	70 new	no
MSS1P7	0.8	150/60	no	-
MSS1P8	2	150/60	70 new	no
MSS1P9	2	150/60	80 old	yes
MSS1P10	2	137/120	80 old	yes
MSS1P11	2	137/120	80 new	yes
MSS1P12	0.8	150/60	80 old	yes
MSS1P13	0.8	137/120	80 new	yes
MSS1P14	2	150/60	no	-
MSS1P15	0.8	137/120	no	-
MSS1P16	2	150/60	70 new	yes
MSS1P17	0.8	150/60	80 old	no
MSS1P18	0.8	137/120	70 new	yes
MSS1P19	0.8	137/120	80 old	no
MSS1P20	2	150/60	80 old	no

MSS1P21	2	137/120	70 new	no
MSS1P22	2	150/60	no	-
MSS1P23	2	137/120	no	-
MSS1P24	0.8	150/60	80 new	no
MSS1P25	2	137/120	70 new	yes
MSS1P26	2	150/60	80 new	no
MSS1P27	0.8	137/120	80 new	no
MSS1P28	2	150/60	80 new	yes
MSS1P29	0.8	150/60	80 new	yes
MSS1P30	0.8	137/120	70 new	no

Moreover, the optimal static strain test parameters were elaborated in several pre-experiments for a representative hose cover material A (c.f. 7.1). In order to balance information gain and experimental time, they were defined as following:

- 30 % strain
- crack assessment interval: 4 hours
- total static strain test time: 120 hours

In addition, the assessment interval was prolonged, after 60 hours exposition time to 8 hours and subsequently to 24 hours, due to slower crack progression.

For the sake of reproducibility all 30 test specimens, prepared from the aforementioned 30 rubber sheets, were subjected parallel to the static strain test in the same ozone chamber. Additionally, all rubber sheets were tested two times for their ozone resistance.

5.1.3 Data analysis

Since the detailed crack assessment was done according to appendix C of ISO 1431-1:2012, the first step was to arrange the possible crack levels according to their impact on the material. Therefore, several assumptions were made: Primarily, if cracks were only visible at the edges of the specimen, the impact was downrated due to the fact that the edges are more likely to be attacked by ozone in comparison to the rest of the surface. Moreover, when looking at hydraulic hoses such edges are not existing. Secondly, it was defined that the length of the ozone cracks has a smaller directly proportional negative impact on the material, than the number of cracks has. It has to be added that for different tasks – with different rubber products – this arrangement has to be reconsidered. Table 7 shows the arranged crack levels and also the translation into a numerical system. This translation was done in order to facilitate a plot of the crack evaluation time against the crack level number (Figure 6).

Table 7: arranged crack assessment levels according to ISO 1431-1:2012 and their translation into a numerical system

crack level acc. standard	numerical crack assessment
1SE	1
2SE	2
3SE	3
1FE	4

2FE	5
3FE	6
1NE	7
2NE	8
3NE	9
1S	10
2S	11
3S	12
1F	13
2F	14
3F	15
1N	16
2N	17
3N	18
material failure	19

A legend for the crack assessment code is displayed in chapter 7.2 (c.f. 7.2, Table 31).
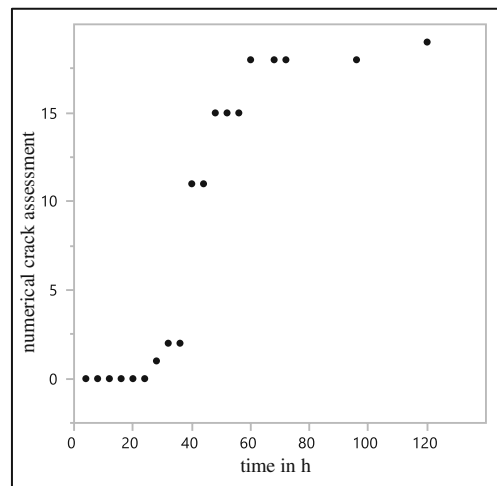
Figure 6: example crack assessment data plot of MSS1P1 repetition 2

In order to perform a proper data analysis in the JMP software, a value was needed that is proportional to the ozone resistance of the rubber sheets. Therefore, different curves were fitted into the data plot (Figure 7), showing that a Gompertz 3P Model (Equation 3) was optimal for the collected data.

In the next step the inflection point of this curve was chosen as value that describes the ozone resistance, of the different rubber sheets, best. The inflection point is directly proportional to the ozone resistance of the rubber sheets; therefore, this value was consequently extracted from the data and is displayed in the Appendix (*c.f.* Table 33). In the last step, the arithmetical mean was calculated from the extracted values of both repetitions. This was done, as it was observed that the second testing cycle showed tendentially higher inflection points. Subsequently, the transformation of variations – that were not implicated, due to changed boundary conditions – on the least square fitting model, resulting in higher error margin, had to be prevented. This

mean inflection point was subjected to a least square fitting in the JMP software. The fitting led to the Pareto-diagram (Figure 8) and the statistically significance (Figure 9).

Equation 3: Gompertz 3P Model; a... asymptote, b... growth rate, c... inflection point

$$y = a * e^{-e^{-b*(x-c)}}$$
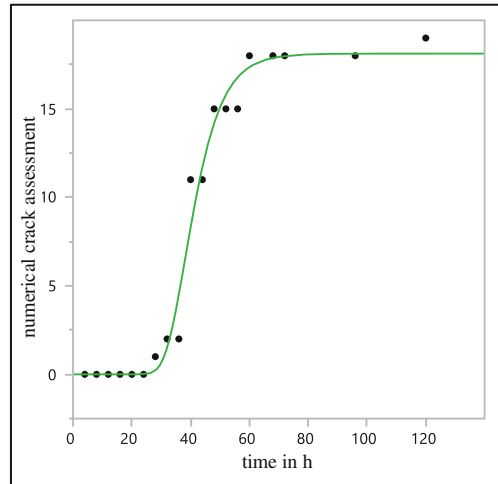
Figure 7: example crack assessment data plot with fitted Gompertz 3P model of MSS1P1 repetition 2

It can be seen that only the specimen's thickness and the tape imprint, but no secondary interactions are statistically significant. In addition, the Pareto diagram shows, that the tape has the biggest negative influence- and thicker specimens the biggest positive influence on the ozone resistance of the rubber sheets.

Term	Orthog Estimate
Tape [yes]	-17.00273
Thickness [2.0 mm]	15.56069
Old tape [yes]	-9.43682
Vulcanization [137°C/120min]	-6.18061
Old tape [yes]*tape overlap [yes]	5.04574
Thickness [2.0 mm]*tape[yes]	-5.03051
Thickness [2.0 mm]*vulcanization[137°C/120min]	-3.67378
Tape [yes]:tape overlap[yes]	-3.02203
Thickness [2.0 mm]*old tape [yes]	-2.97315
Tape [yes]:tape width[70mm]	2.28893
Tape [yes]:tape overlap[yes]*vulcanization[137°C/120min]	-1.24900
Tape [yes]:tape overlap[yes]*tape width[70mm]	-1.02959
Vulcanization [137°C/120min]*old tape [yes]	-0.87306
Tape [yes]:tape width[70mm]* vulcanization[137°C/120min]	-0.64054
Vulcanization [137°C/120min]* tape [yes]	0.50237
Tape [yes]:tape overlap[yes]*thickness [2.0 mm]	0.26490
Tape [yes]:tape width[70mm]* thickness [2.0 mm]	-0.07511

Figure 8: Pareto plot of transformed estimates

The indication ":" between two factors imply that they are nested, e.g. without the application of a tape the factor "old tape" cannot exist.

Source	LogWorth		PValue
Tape	2.694		0.00202
Thickness	2.448		0.00356
Old tape*tape overlap	0.997		0.10060
Thickness*tape	0.962		0.10905
Thickness*old tape	0.680		0.20871
Old tape	0.647		0.22544 ^
Vulcanization	0.555		0.27893
Tape width[tape]	0.490		0.32371
Thickness*vulcanization	0.481		0.33049
Tape overlap[tape]	0.279		0.52637
Tape overlap*vulcanization[tape]	0.241		0.57423
Vulcanization*old tape	0.161		0.68963
Tape overlap*tape width[tape]	0.156		0.69805
Tape width*vulcanization[tape]	0.091		0.81125

Figure 9: effect summary (significance)

Arithmetical Mean Predicted RMSE=11.379 RSq=0.94
PValue=0.0005
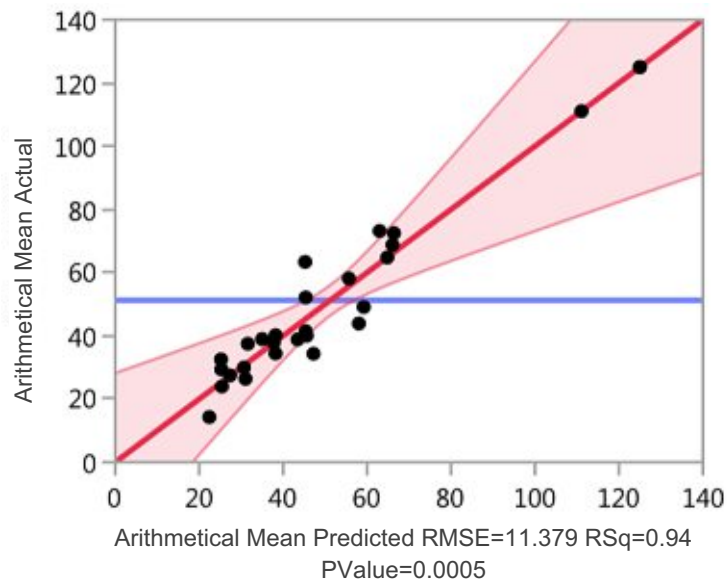
Figure 10: actual by predicted plot

Arithmetical Mean Predicted
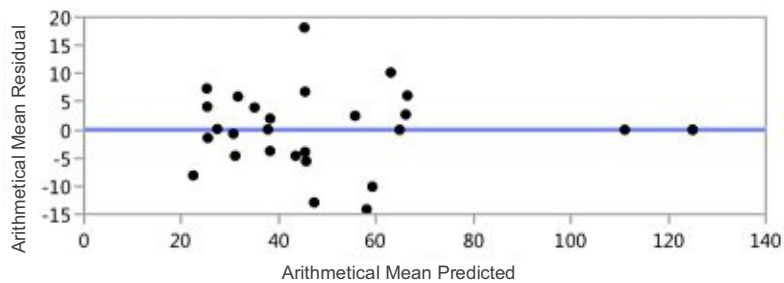
Figure 11: residual by predicted plot

Table 8: summary of fit

description	value
RSquare	0.94
RSquare Adj	0.84
Root Mean Square Error	11.38
Mean of Response	51.23
Observations	28
AICc	320
BIC	250

In Figure 10 the actual by predicted plot – with a RMSE of 11.38 and a PValue of 0.0005 – gives an overview how good the fitted model predicts the measured values by plotting predicted values (X-axis) against measured values (Y-axis). The closer these points are to the X=Y diagonal the better is the goodness-of-fit. In addition, the residual by predicted plot is shown in Figure 11, the residues are randomly distributed around the center line and show no pattern. The in Table 8 summarized data shows further characteristics of the fit and with RMSE, AICc and BIC giving data for model comparison.

The negative influence of the tape imprint on the ozone resistance of the rubber may be due to the following reasons: Obviously this three-dimensional surface structure increases the surface area drastically, accelerating the ozone attack and therefore facilitating the crack formation. During the removal of the nylon tape the surface may suffer from micro damages, again resulting in a faster ozone attack.

Looking at the negative influence of the thinner thickness on the ozone resistance, it may be attributed to the fact that the surface to bulk ratio is increased and therefore surface attacks have a more severe effect on the material.

It has to be added that not for all rubber sheets the Gompertz 3P Model could be fitted into the datapoints. For instance, when looking at rubber sheets with a high resistance to ozone cracks (e.g. MSS1P14, MSS1P22 and MSS1P23), where no cracks were visible during the whole time of the experiment, the inflection point was set to 125 hours. The data of plate MSS1P8 repetition 1 and MSS1P15 repetition 2 was, due to the fact that the Gompertz 3P Model could not be fitted, omitted. For these two plates no arithmetical mean was calculated.

All raw data of the two replication measurements is shown in Table 34 and Table 35 in the appendix (*c.f.* Appendix). In addition, there are also microscopic pictures of plate MSS1P17 (*c.f.* Figure 22, Figure 23) and plate MSS1P18 (*c.f.* Figure 21) after 24 hours static ozone test shown.

5.1.3.1 Limitations

The recreation of the hydraulic hose production parameters on the laboratory test specimen entails several deviations. During the wrapping of the hydraulic hoses with the nylon tape, a defined strain is applied on the tape. This strain could not be replicated accurately, due to the use of a hydraulic press for the specimen's vulcanization (*c.f.* Appendix, Figure 25 and Figure 26). In addition, the hydraulic press applies a pressure of approx. 320 bar during the

vulcanization process of the rubber sheets. This high pressure is not applied during the hose's production.

The used crack assessment does not display the spatial distribution of the cracks. Therefore, the statistical evaluation omits the fact that in the deepening – produced from the tape overlap – a crack cumulation was observed, not necessarily worsening the crack level. This phenomenon was reported especially during the first repetition of the experiment; however, it was not that distinct during the second duplication of the experiment. In order to investigate this observation additionally, more detailed experiments have to be conducted.

In some cases, before the first crack on the surface showed up, a total material failure occurred (*c.f.* Appendix, Table 34 (e.g. MSS1P13 and MSS1P29) and Table 35 (e.g. MSS1P7)). The material broke near the clamp mounting point. This behavior made a crack progress monitoring and therefore a fine segmented information gathering, in these special cases, impossible. Due to the fact that it is unknown why some rubber sheets showed this behavior, the data could not be omitted for the statistical analysis. This observation was made not only on rubber sheets with a low ozone resistance, but also with a medium and good resistance to ozone cracks.

The second most frequent starting point of the aforementioned total material failure was the deepening in the surface, due to the – in some sheets – applied tape overlap.

5.2 Surface modification

All surface modifications were primary tested with material B (*c.f.* 7.1), if additional materials were tested it is separately stated.

5.2.1 Ozone pre-passivation

As already mentioned in chapter 3.5.2.1 (*c.f.* 3.5.2.1) an ozone pre-passivation was believed to be a possible strategy against further ozone attacks on the modified rubber, even under strain. Since the degradation of rubber is a surface process, it was assumed that, if the reaction of the surface double bonds leads to a reduction of the same, the ozone resistance of the rubber could be improved. To underpin this theory the possible effect was systematically investigated. Therefore, the ozone concentration and the reaction time of unstrained rubber with ozone was varied (Table 32). However, during these experiments the temperature and the relative humidity were hold constant to 30 °C and 55 % RH. If a positive effect at defined passivation conditions could be reported, the experiment was repeated two additional times.

In the beginning of these passivation experiments, concentrations of 10 pphm and 50 pphm were used with reaction times between 1- and 7-hours. Since this first data showed no change in the ozone resistance of the test material, further tests with 10- and 30-minutes, and 24-, 96- and 168-hours reaction time were conducted. This was done in order to exclude a possible overreaction resulting in a degradation instead of a passivation or an incomplete reaction leaving reactive double bonds behind. However, these additional experiments showed no positive effect on the ozone resistance neither.

In the next step it was tried to increase the bimolecular reaction rate between ozone and the rubber double bonds (*c.f.* 3.4), hence the ozone concentration was increased to 200 pphm. Again, different reaction times between 1- and 96-hours were screened, showing little enhancements for 1-, 2-, 4- and 96-hours and no effect with 8- and 24-hours reaction time (Table 13). These data are rather surprising, since the ATR/FT-IR showed a constant increase of the carbonyl band and a constant decrease of the double-bond band with increasing reaction time (Figure 12), suggesting a constant improved passivation with reaction time.

Since it is known that the ozone degradation of rubber is directly proportional to the relative humidity (*c.f.* 3.4), a last attempt was made and the test specimen were passivated at 80 % RH, 200 pphm for 1- to 8-hours. At these conditions no passivation effect was observed at all, thus the pre-passivation evaluation was ceased.

It has to be added that the surface reaction could not only be tracked by physical and chemical characterizations, but also due to surface staining (greenish shimmer, *c.f.* Figure 24) and haptic changes (sticky surface).

Additionally, to the earlier mentioned ATR/FT-IR measurements, which gather information in a depth of approx. 2-3 µm, XPS and SFE characterizations were conducted, in order to reveal information of the outermost nanometers of the material (Table 10; Table 11 and Table 12).

Reasons for the insufficiency of this passivation method could have manifold origins. The observed stickiness of the modified surface could elucidate the presence of macromolecules with low molecular weight, which formed due to polymer chain cleavage during the reaction with ozone. This cleaving process would therefore constantly expose new surface double bonds. Another possible explanation could be an increase in surface roughness during the

passivation reaction leading to a higher surface area and thus even accelerating the ozone attack after strain is applied to the material.[54, 55]
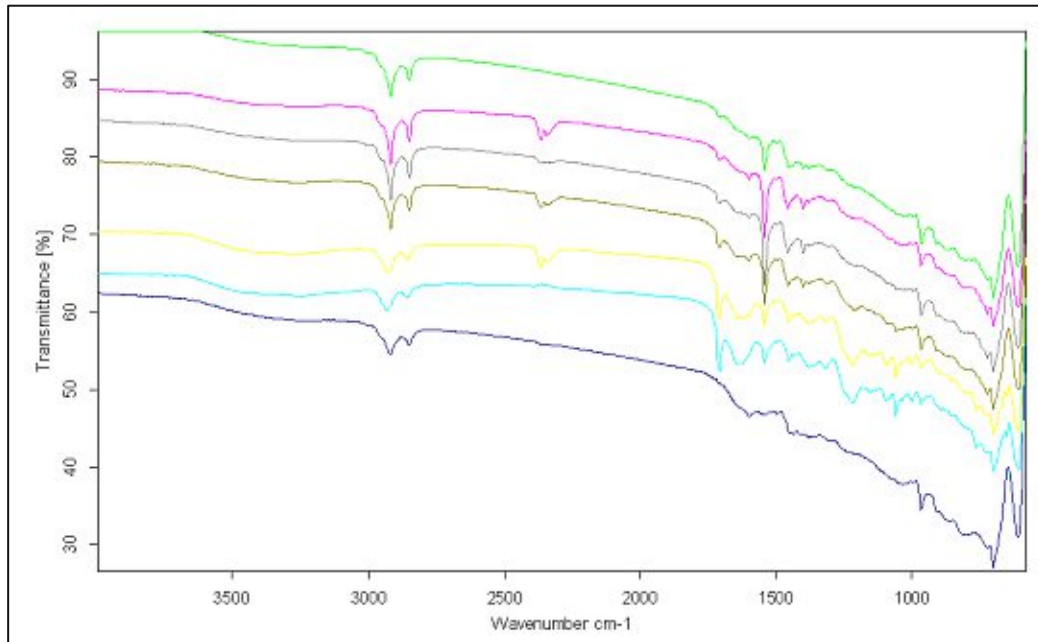
Figure 12: ATR/FT-IR spectra; from top to bottom: 1-, 2-, 4-, 8-, 24-, 96-hours reaction time with 200 pphm ozone and 55 % RH; undermost trace depicting the blank measurement of the unmodified test specimen

Table 9: IR bands

band wavenumber in cm^{-1}	possible origin	wavenumber literature[54] in cm^{-1}
3500 (very broad)	-OH stretching	3450
2917	C-H butadiene	2919
2848		2851
1705	carbonyl	1717
1640	H_2O surface	1650
1544	Zn-Stearate	1540
1220	C-O-C	1190
962	C=C	968

Table 10: solid free energy measurements of pre-passivated rubber samples (200 pphm ozone concentration, 55 % RH, 30 °C)

reaction time in hours	SFE overall in mN/m	disperse part in mN/m	polar part in mN/m
0 (blank)	24.65 ± 2.18	24.63 ± 2.15	0.02 ± 0.06
1	27.77 ± 1.85	27.75 ± 1.81	0.02 ± 0.04
2	29.18 ± 1.09	29.16 ± 1.00	0.02 ± 0.08
4	28.86 ± 2.56	28.84 ± 2.47	0.02 ± 0.09
8	30.23 ± 1.44	30.14 ± 1.24	0.09 ± 0.19

Looking at the surface free energy data, one can see a significant increase between the blank and the modified samples in the disperse part of the SFE. The polar part is unchanged by the

modifications and there is also hardly any increase in the disperse part to be reported with increasing reaction time.

Specimens with a reaction time of 8- and 24 hours were subjected to XPS analysis. These measurements revealed the detailed composition of the modified surface which is depicted in following tables.

Table 11: XPS survey, quantification of pre-ozonated rubber samples (200 pphm ozone concentration, 55 % RH, 30 °C)

reaction time in hours	Ar sputtering in s	at%					
		C	N	O	S	Zn	Na
blank	0	86.8	-	11.3	-	0.3	-
	180	92.5	4.4	1.1	1.5	0.5	-
	780	93.9	3.9	1.6	05	0.1	-
8	0	90.6	-	9.1	-	0.3	-
	180	90.1	3.4	3.4	1.1	0.6	1.4
	780	92.6	3.6	2.8	0.7	0.2	0.2
24	0	80.0	2.8	16.8	-	0.4	-
	180	91.1	2.0	3.1	3.2	0.6	-
	780	93.1	3.6	1.8	1.3	0.2	-

Table 12: XPS detail C1s spectrum data of pre-ozonated rubber samples (200 pphm ozone concentration, 55 % RH, 30 °C)

reaction time in hours	Ar sputtering in s	at%				
		blank	charging	C-C/C-H	C-O	C=O
8	0	96.9	3.1	-	-	-
	180	88.7	-	8.7	2.5	-
24	0	89.2	2.9	-	5.7	2.1
	180	93.7	-	4.8	1.5	-

All detected elements and groups are in line with the expectations, which were made based on the rubber recipe and the surface modification. When looking at the XPS survey data (Table 11), the O content of the longer modified sample (24 hours) in the as received state is increased, in comparison to the blank. After the surface was sputtered with argon, the O content is significantly reduced in all samples. Moreover, the aforementioned difference between the distinctive modification times was lost. This may be due to the fact that the elastomer does not withstand the Argon sputtering event. Further measurements were therefore limited to 0- and 180-second sputtering time.

Looking at the S, N, Zn and Na content, no significant trend could be reported regarding reaction time or sputtering time.

Table 12 shows the data of the C1s spectrum, which are expressed in relation to the blank. Therefore, the column "blank" shows the percentage of the treated sample, which is equal to the blank. Again, the longer treated sample shows further O components (C-O and C=O), but also charging effects come into action. The charging effects make interpretations of the C1s spectrum troublesome and sometimes even not possible. This problem might be eliminated when using a more sophisticated spectrometer.

However, the findings underline the existence of an ozonated rubber layer, which was also discovered in ATR/FT-IR measurements.

Additionally, a O1s spectrum was measured, but showed no significant differences compared to the blank. All XPS-spectra and binding energy tables are shown in the appendix (*c.f.* Table 36, Table 37 and Figure 27 following).

Table 13: static strain test data pre-passivation (200 pphm ozone concentration, 55 % RH, 30 °C); 10 % strain, 96 hours conditioning at rt, 50 pphm ozone, 55 % RH, 40 °C

reaction time in hours	crack assessment time in hours					
	1	**2**	**3**	**5**	**9**	**25**
blank	2F	2N	3N	3N	3N	3N
	2S	2N	2N	3N	3N	3N
	2S	2F	3F	3F	3F	3N
1	0	1SE	2S	3S	3S	3F
	0	1SE	2S	3S	3S	3S
	0	1SE	2S	3S	3S	3F
2	0	1SE	2SE	3SE	3S	3F
	0	1SE	2SE	3S	3S	3S
	0	1S	2S	3F	3F	3N
4	1SE	2SE	2S	3S	3S	3F
	0	1SE	2SE	3S	3S	3S
	0	1S	2S	3F	3F	3N
8	1SE	2S	2S	3S	3S	3N
	1S	2S	2S	3F	3F	3F
	1S	2S	2N	3N	3N	3N
24	1F	2N	2N	3N	3N	3N
	1S	2F	2N	2N	3N	3N
96	0	0	2S	2S	3S	3S

5.2.2 Catalyzed oxidation

As proposed in literature[33] a controlled surface oxidation may affect the ozone resistance of rubber in a positive way. To investigate this phenomenon three samples were oxidized under a UV lamp for 2-, 6.5- and 24-hours. Unfortunately, these early experiments showed no significant impact on the ozone resistance. In order to catalyze the reaction, as depicted in chapter 3.5.2.2 (*c.f.* 3.5.2.2) and also in literature[33], $CuCl_2$ was applied to the surface prior to the UV treatment. This was done by dipping the rubber specimen into an ethanolic solution of $CuCl_2$ for different time spans (30- and 60-sec. and 1 h). The following UV treatment was applied for 0-, 2-, 6- and 24-hours. These modifications result in an altered crack pattern, as the material mainly cracked at the edges. When looking at the crack assessment data (Table 14) it appears that the positive impact is not only visible at the UV treated samples, but also when only copper chloride was applied. Moreover, no trend with increased UV exposure time was noticeable. This effect may be based on copper residues, which if oxidized to copper oxide show a catalytic activity for the ozone decomposition. Thus decelerating the attack rate on the

rubber surface.[33] Since the specimen were always cleansed after the completion of the modifications, the observed effect is a matter of a small copper amount.

Due to the aforementioned effect, the fact that the rubber oxidation can also result in a chain scission and the circumstance that copper is a rubber poison, the catalytical oxidation approach was abandoned.

Table 14: static strain test data catalyzed oxidation; 10 % strain, 96 hours conditioning at rt, 50 pphm ozone, 55 % RH, 40 °C

reaction conditions	crack assessment time in hours					
	1	**2**	**3**	**5**	**9**	**25**
blank	0	2S	2S	2F	3F	3N
2 h UV	1S	2F	2N	3N	3N	3N
6.5 h UV	1SE	2S	2S	3F	3F	3F
24 h UV	0	1SE	1S	2S	3S	3S
30 s CuCl$_2$/0 h UV	0	0	0	0	0	2S
60 s CuCl$_2$/0 h UV	0	0	0	0	0	2S
1 h CuCl$_2$/0 h UV	0	0	0	1SE	2SE	2SE
30 s CuCl$_2$/2 h UV	0	0	1S	1S	2S	3S
60 s CuCl$_2$/2 h UV	0	0	2S	2S	2S	3S
1 h CuCl$_2$/2 h UV	0	0	0	2SE	2FE	3FE
30 s CuCl$_2$/6 h UV	0	0	0	2SE	2SE	3SE
60 s CuCl$_2$/6 h UV	0	2S	2S	2S	2S	3S
1 h CuCl$_2$/6 h UV	0	0	1SE	2FE	2FE	3FE
30 s CuCl$_2$/24 h UV	0	0	1S	2S	2S	3S
60 s CuCl$_2$/24 h UV	0	0	0	2SE	2SE	3SE
1 h CuCl$_2$/24 h UV	0	0	0	2FE	2FE	3FE

5.2.3 Dihydroxylation

The aforementioned (*c.f.* 3.5.2.3) dihydroxylation reaction was tested with three different reaction times (30 sec, 60 sec and 1 h) for its possible positive impact on the ozone resistance of rubber. After the modification was done the specimen's surface was reported to be smoother and less adherent. Moreover, the longest reaction time led to a grainy surface with loosely attached carbon black. Only the specimen with the longest modification time exhibited a significant positive alteration of the ozone resistance (Table 15). However, with this long reaction time also a surface destruction was visible, maybe due to chain scissions. To avoid these chain scissions and perform only the desired dihydroxylation reaction, the reaction kinetic had to be improved. Therefore, the temperature was lowered to 5 °C for the following reactions and furthermore the reaction times were changed to 1-, 10- and 60-minutes. The new modified samples showed the same haptic changes as earlier mentioned, but the longest reaction time presented a less destructed surface. Unfortunately, the ozone resistance was not changed significantly (Table 15). Thus, this surface modification was abandoned.

Table 15: static strain test data dihydroxylation; 10 % strain, 96 hours conditioning at rt, 50 pphm ozone, 55 % RH, 40 °C

reaction conditions	crack assessment time in hours					
	1	**2**	**3**	**5**	**9**	**25**
blank	1S	2N	2N	3N	3N	3N
rt; 30 sec	2S	2F	2F	2N	3N	3N
rt; 60 sec	2S	2F	2F	2N	3N	3N
rt; 1 hour	0	1SE	1SE	1FE	2S	3F
5 °C; 1 min	2F	2N	2N	2N	3N	3N
5 °C; 10 min	2F	2N	2N	3N	3N	3N
5 °C; 1 hour	2FE	2N	2N	3N	3N	3N

5.2.4 Chlorination

As mentioned in chapter 3.5.2.4 (*c.f.* 3.5.2.4) there are some hints in literature, that surface chlorination reactions of rubber lead to an improved ozone resistance. Since in the production of powder free latex gloves aqueous NaOCl solution (13 %) and conc. HCl is used, these chemicals were also applied in this thesis. The experiments were started with three different reaction times (1-, 10- and 60-min) and were repeated three times, whereupon the shortest reaction time proved to be sufficient. The specimen with 1 min of modification time showed for 3-9 hours no crack during the static strain test. In comparison the unmodified blank showed already cracking below one hour, when 10 minutes reaction time were applied there was no crack visible for 1-5 hours and with 60 minutes, the time without cracks was reported to be 1-3 hours (Table 19).

The stated trend of a decreasing positive effect on the ozone resistance of the rubber with increasing reaction time might be attributed to a formation of microcracks on the surface, which was reported in literature.[56] This crack formation behaves directly proportional to the reaction time and facilitates the ozone attack, due to a bigger surface area, and therefore accelerating the ozone degradation.
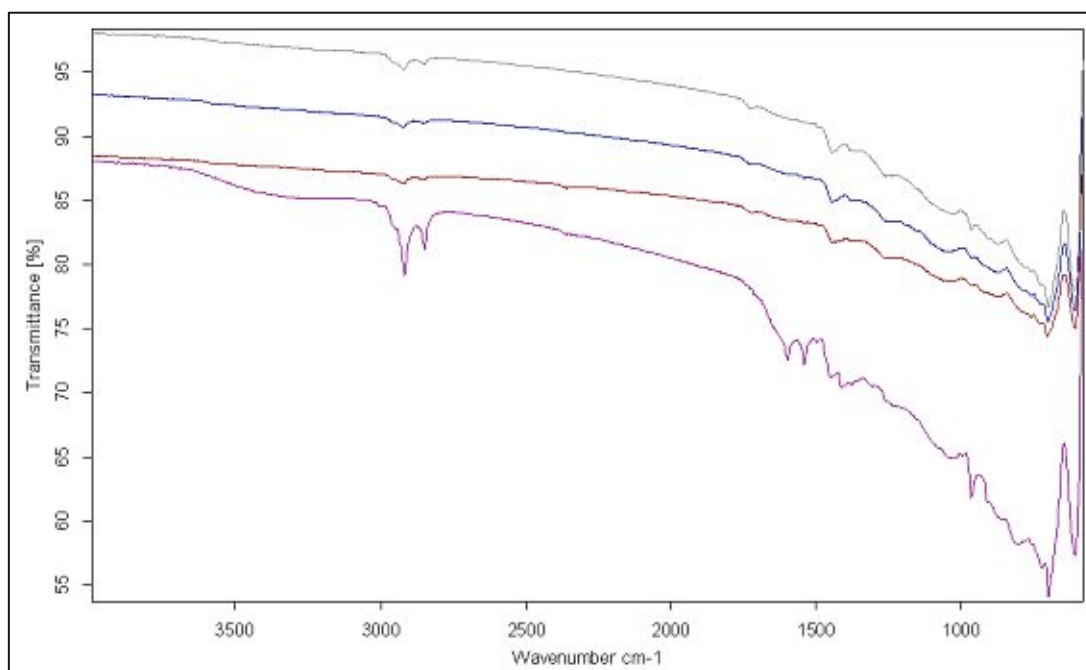
Figure 13: ATR/FT-IR spectra; from top to bottom: 1-, 10-, 60-min reaction time; chlorinated samples (acidified aqueous NaOCl solution (13 %)); undermost trace depicting the blank measurement of the unmodified test specimen

The intensity of IR signals of the measured chlorinated samples was not satisfying, although it can be said that the C-C-double bond band (~960 cm^{-1}) decreases drastically with longer reaction times (Figure 13). The C-Cl vibration is not visible, since there were some overlaps at the lower wavenumbers (<800 cm^{-1}).

Table 16: solid free energy measurements of chlorinated rubber samples (acidified aqueous NaOCl solution (13 %))

reaction time in min	SFE overall in mN/m	disperse part in mN/m	polar part in mN/m
0 (blank)	24.65 ± 2.18	24.63 ± 2.15	0.02 ± 0.06
1	38.86 ± 2.24	36.04 ± 1.59	2.83 ± 0.64
10	42.25 ± 3.66	35.16 ± 1.90	7.09 ± 1.77
60	40.68 ± 3.06	35.39 ± 1.93	5.29 ± 1.13

As can be seen in Table 16 one minute of reaction time is sufficient to raise the SFE, especially the disperse part, significantly. Longer reaction times have additional impact on the polar part of the SFE, the disperse part is unchanged in comparison to one-minute reaction time.

Table 17: XPS survey, quantification of chlorinated rubber samples (acidified aqueous NaOCl solution (13 %))

reaction time in min	Ar sputtering in s	C	N	Cl	O	S	Zn	Na
					at%			
blank	0	86.8	-	-	11.3	-	0.3	-
	180	92.5	4.4	-	1.1	1.5	0.5	-
1	0	85.9	1.6	2.1	10.0	-	0.4	-
	180	92.7	1.8	3.6	1.7	-	0.2	-
10	0	81.2	1.4	5.9	10.1	-	0.4	-
	180	87.8	2.6	7.3	1.8	-	0.2	0.2

Table 18: XPS C1s detail spectrum of chlorinated rubber samples (acidified aqueous NaOCl solution (13 %))

reaction time in min	Ar sputtering in s	at%				
		blank	charging	O-C=O	C-Cl	C=O
1	0	89.2	0.0	-	8.1	2.1
	180	92.8	-	2.8	4.4	-
10	0	58.7	26.1	-	13.4	1.7
	180	92.9	-	2.5	4.6	-

The XPS survey data (Table 17) clearly shows the installation of Cl on the rubber surface. The elements N, O, S, Zn and Na are not changed due to this surface modification. Ar sputtering increases the relative Cl content for both treatment times. This increase is based on the sharply dropping O content after Ar sputtering, as also mentioned in chapter 5.2.1 (*c.f.* 5.2.1).

When looking at the detailed C1s spectrum (*c.f.* Figure 32) the longer reaction time shows a strong peak broadening, which may be based on charging effects. However, the relative content of the C-Cl group is clearly increasing. The mentioned charging effect is mainly reported where more intense surface modifications were conducted and may occur due to changes in the electronic properties of the material. The reason for the transformation of the C=O groups to O-C=O groups – due to Ar-sputtering – is unknown at this point.

Table 19: static strain test data chlorination; 10 % strain, 96 hours conditioning at rt, 50 pphm ozone, 55 % RH, 40 °C

reaction time in min	crack assessment time in hours								
	1	2	3	5	9	25	49	73	97
blank	1S	2F	2F	2N	3N	3N	-	-	-
	2N	2N	2N	3N	3N	3N	-	-	-
	1N	2N	2N	2N	3N	3N	3N	3N	3N
1	0	0	0	2S	2S	2F	-	-	-
	1S	2S	2S	2F	2F	3F	-	-	-
	0	0	0	0	0	2SE	2SE	3S	3S
10	0	2S	2S	2S	2S	2S	-	-	-
	1S	2S	2S	2S	2S	3F	-	-	-
	0	0	0	0	2SE	2FE	2FE	3FE	3FE
60	0	2S	2S	2S	2S	2S	-	-	-
	1S	2S	2S	2S	2S	2F	-	-	-
	0	0	0	1SE	2SE	2FE	2FE	3FE	3F

Additionally, it could be reported that the surface chlorination – at least at short reaction times – has a comparable positive effect (Table 20) on material C (*c.f.* 7.1).

Table 20: static strain test data chlorination of material C; 10 % strain, 96 hours conditioning at rt, 50 pphm ozone, 55 % RH, 40 °C

	crack assessment time in hours					
reaction time in min	**1**	**2**	**3**	**5**	**9**	**25**
blank	1S	2F	2F	2N	3N	3N
1	0	0	0	2S	2S	2S
10	0	2S	2S	2S	3F	3N
60	2S	2S	2S	3S	3S	3N

5.2.5 Epoxidation

5.2.5.1 Approach A (NaOCl/KBr)

Epoxidation reactions are a common method to modify rubber and therefore alter its chemical properties. This modification is normally applied on raw rubber.[4] Additionally, epoxidation reactions depict a crucial part in organic chemistry, as mentioned earlier (*c.f.* 3.5.2.5). First attempts were conducted with aqueous basic NaOCl solution (13 %; pH ≈ 10) as oxidizing agent and lead to no significant and/or reproducible effect on the rubber specimens. In order to increase the reactivity of the oxidizing agent 1.5 equiv. of KBr were added, in order to form the hypobromite *in-situ,* as depicted in chapter. 3.5.2.5 (*c.f.* 3.5.2.5).

The reaction was tested with different reaction times (1-, 10-, 60-, 120-minutes) and since the first reaction cycle showed a significant improvement on the ozone resistance of the rubber samples, the reaction was repeated twice in order to demonstrate a reproducible effect. The optimum was found at a reaction time of 1 hour, at least doubling the time until the first crack is visible in comparison to the unmodified specimen (blank). For further insights into the exact crack assessment data see Table 22. The reaction time of two hours showed severe surface alterations, since after a visual inspection the roughness seemed to be increased and it was also observed that carbon black was only loosely bond to the surface. These observations indicate that the polymer network might be destroyed at some point, due to the rather harsh epoxidation reaction. The altered surface made a serious crack assessment nearly impossible, due to visibility problems of the cracks, especially in early stages. Therefore, the data for this last modification may be biased.

Additionally, the orange staining of the reaction solution could indicate the formation of Br_2. Further XPS investigations might clarify the exact surface modification of these experiments.
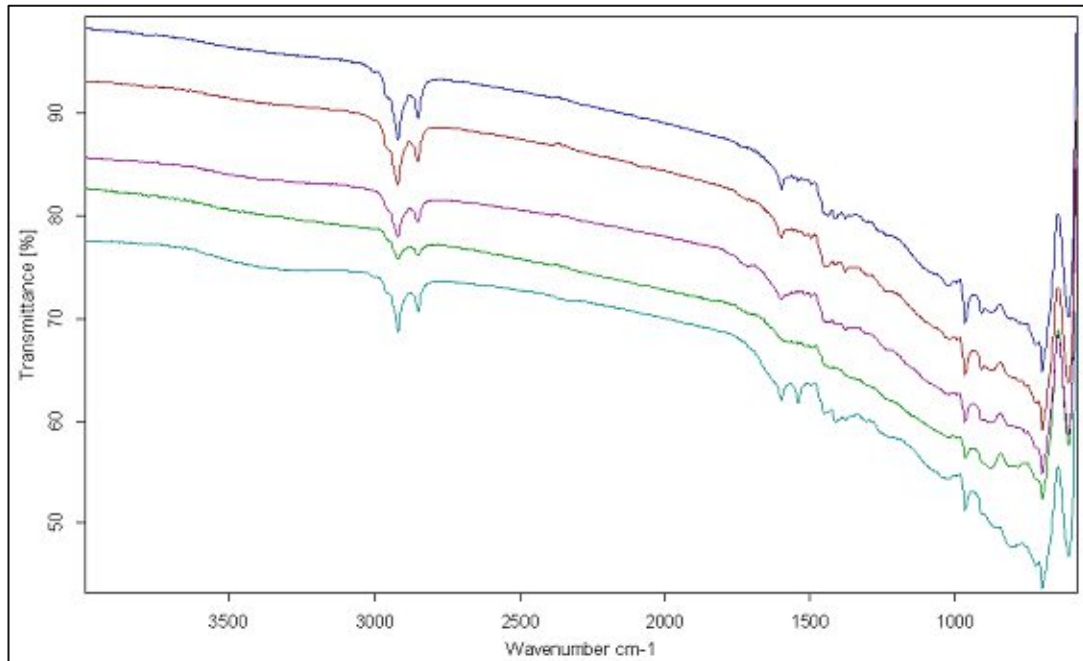
Figure 14: ATR/FT-IR spectra; from top to bottom: 1-, 10-, 60-, 120-min reaction time; 93.5 g KBr in aqueous 13 % NaOCl solution; undermost trace depicting the blank measurement of the unmodified test specimen

Looking at the ATR/FT-IR spectra in Figure 14 it can be clearly seen that not only the C-C-double bond band at approx. 960 cm^{-1}, but also the polymeric bands decrease proportional to the reaction time. This intensity loss effect might be due to an enrichment of loosely bond carbon black on the surface.

Table 21: solid free energy measurements of epoxidized rubber samples (93.5 g KBr in aqueous 13 % NaOCl solution)

reaction time in min	SFE overall in mN/m	disperse part in mN/m	polar part in mN/m
0 (blank)	24.65 ± 2.18	24.63 ± 2.15	0.02 ± 0.06
1	24.61 ± 2.45	24.29 ± 2.06	0.32 ± 0.39
10	27.04 ± 1.78	25.98 ± 1.18	1.05 ± 0.60
60	30.61 ± 2.33	30.13 ± 1.96	0.48 ± 0.37
120	51.73 ± 2.26	47.27 ± 1.29	4.46 ± 0.98

The experiment with a reaction time of one minute has no impact on the surface free energy (Table 21). 10- and 60-min reaction time show an increased disperse part and hardly any change in the polar part. The experiment with 120 min reaction time shows a strong elevation in the SFE overall. Yet this increase may be due to the earlier mentioned carbon black enrichment in the surface region.

Table 22: static strain test data epoxidation A; 10 % strain, 96 hours conditioning at rt, 50 pphm ozone, 55 % RH, 40 °C

reaction time in min	crack assessment time in hours								
	1	**2**	**3**	**5**	**9**	**25**	**49**	**73**	**97**
blank	1N	2N	2N	2N	3N	3N	3N	3N	3N
	0	2N	2N	2N	3N	3N	3N	-	-
	1N	2N	2N	3N	3N	3N	-	-	-
1	1F	2N	2N	2N	3N	3N	3N	3N	3N
	0	2S	2S	2F	2N	3N	3N	-	-
	0	2F	2F	2F	2N	3N	-	-	-
10	1S	1S	2S	2S	3S	3F	3F	3N	3N
	0	2S	2F	2F	2N	3N	3N	-	-
	0	2S	2S	2F	2F	3N	-	-	-
60	0	0	2S	2S	3S	3S	3F	3F	3F
	0	1S	1S	2S	2F	3F	3N	-	-
	0	1S	2S	2S	2F	3F	-	-	-
120	0	0	0	1SE	2FE	2FE	3NE	3NE	3NE
	0	0	1S	2S	2S	3F	3N	-	-
	0	0	0	2S	3S	3S	-	-	-

5.2.5.2   Approach B (m-CPBA)

Approach A (5.2.5.1) showed the potency of surface epoxidation reactions on cured rubber, regarding a positive impact on the ozone resistance of rubber. In order to use less harsh reaction conditions and with indications in the literature[45], showing functioning epoxidation reactions on the rubber surface, the oxidizing agent was changed to m-CPBA. Since this substance is insoluble in water, 2-propanole was used as reaction medium. General advantages of m-CPBA are listed in chapter 3.5.2.5 (*c.f.* 3.5.2.5).

The reaction time was varied between 1-minute and 18-hours in order to screen for the optimal conditions. All experiments were conducted three times.

One minute of reaction time seemed not to be sufficient, but even this short interval leads at least to a doubling of the time until the first crack is visible in comparison to the unmodified surface, hence achieving the same performance as the best result of previously discussed epoxidation approach A. Further experiments with longer reaction times showed excellent results: When modifying the rubber surface for 10 minutes, no crack was visible during the static strain test for 25 to 73 hours, depending on the repetition. 60 minutes lead to a crack free period of 73 hours and 270 minutes result in 49-96 hours until the first crack appeared. In comparison the untreated blank showed a time without cracks below one hour (Table 26).

It has to be added that the first crack on samples with 10-, 60- and 270-minutes modification time happened instantly as a total material failure. The material broke near the clamp mounting point. This behavior might be due to the higher strain at the mounting point, making the ozone attack more severe. Additionally, the high ozone resistance of the modified material allows no stress relaxation (*c.f.* 3.4), which could decrease the applied strain over time.

Moreover, it could be reported that with increasing reaction time, starting at 10 minutes, the rubber becomes more brittle. Using a reaction time of 270 minutes and more the material loses

nearly all its elastic features, additionally the surface completely breaks open and even partially separates from the bulk. Balancing the positive effect on the ozone resistance against the negative influence on the crucial elastic properties of the rubber material 10 minutes reaction time seem to be the best compromise within evaluated reaction conditions.

This embrittling effect may be also attributed to the used reaction solvent and its possible swelling effect on the rubber, enabling a deeper penetration of the oxidizing agent and thus alteration of the bulk properties.
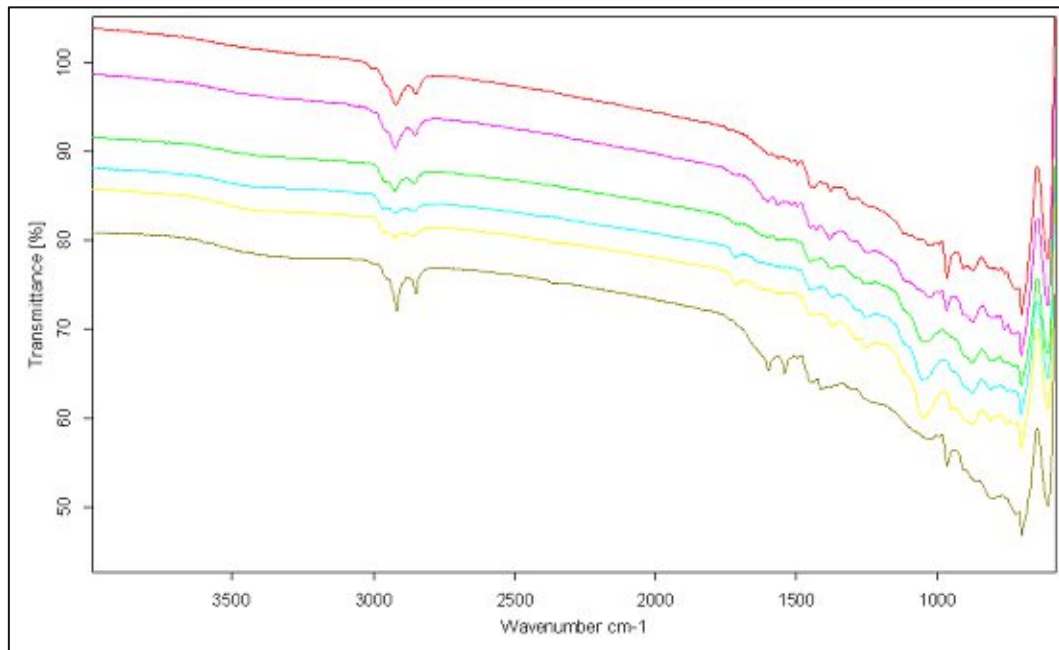
Figure 15: ATR/FT-IR spectra; from top to bottom: 1-, 10-, 60- and 270-min, and 18 h reaction time; 30 % m-CPBA in 2-propanole; undermost trace depicting the blank measurement of the unmodified test specimen

As visible in Figure 15 the C-C-double bond band (~960 cm^{-1}) clearly decreases with reaction time and vanishes at 60 min reaction time. Moreover, at this reaction time the intensity of the polymeric bands also decreases, this behavior cannot be explained at this time. Contrary to this intensity decrease the bands at ~1250 cm^{-1} (epoxy ring stretching[57]), ~870 cm^{-1} (epoxy ring deformation symmetric and/or asymmetric[57]) and 1040 cm^{-1} (probably C-O, stretch[54]) increase.

Table 23: solid free energy measurements of epoxidized rubber samples (30 % m-CPBA in 2-propanole)

reaction time in min	SFE overall in mN/m	disperse part in mN/m	polar part in mN/m
0 (blank)	24.65 ± 2.18	24.63 ± 2.15	0.02 ± 0.06
1	28.73 ± 3.50	27.84 ± 2.71	0.88 ± 0.79
10	30.56 ± 2.99	29.49 ± 2.16	1.07 ± 0.83
60	39.64 ± 4.14	34.33 ± 2.32	5.32 ± 1.82
270	38.40 ± 3.41	33.84 ± 1.64	4.56 ± 1.78

SFE data in Table 23 reveals that even after only one-minute reaction time the disperse part of the SFE is increasing, moreover between 10 and 60 minutes the SFE rises again. This time the polar part is raising too.

Table 24: XPS survey, quantification of epoxidized rubber samples (30 % m-CPBA in 2-propanole)

reaction time in min	Ar sputtering in s	at%					
		C	N	O	S	Zn	Na
blank	0	86.8	-	11.3	-	0.3	-
	180	92.5	4.4	1.1	1.5	0.5	-
1	0	81.0	2.0	14.8	2.0	0.2	-
	180	95.3	1.8	2.0	0.8	0.1	-
10	0	76.3	1.2	20.7	1.4	0.4	-
	180	90.1	4.0	4.4	1.2	0.2	0.1

Table 25: XPS C1s detail spectrum analyses of epoxidized rubber samples (30 % m-CPBA in 2-propanole)

reaction time in min	Ar sputtering in s	at%				
		blank	charging	O-C=O	C-O	C=O
1	0	87.3	-	-	11.2	1.5
	180	95.3	-	1.6	3.1	-
10	0	35.1	51.5	-	12.3	1.0
	180	88.7	-	2.7	8.5	-

According to the XPS survey data (Table 24) the surface epoxidation drastically increases the O content of the surface. This increase seems to be directly proportional to the reaction time and does not affect the relative content of other elements.

The data of the detailed C1s spectrum (Table 25) confirms the formation of epoxy groups – with the showing of C-O moieties – which were also found in the ATR/FT-IR spectrum. Longer sputtering times only result in the harmonization of the different reaction times and therefore point to the possible destruction of the modified surface layer which was mentioned already (*c.f.* 5.2.1).

Table 26: static strain test data epoxidation B; 10 % strain, 96 hours conditioning at rt, 50 pphm ozone, 55 % RH, 40 °C

reaction time in min	crack assessment time in hours								
	1	**2**	**3**	**5**	**9**	**25**	**49**	**73**	**97**
blank	0	2N	2N	2N	3N	3N	3N	3N	3N
	1N	2N	2N	3N	3N	3N	3N	3N	3N
	1S	2F	2N	2N	3N	3N	3N	3N	3N
1	0	0	1S	2S	2S	3S	3F	3N	3N
	0	0	2S	2S	2S	3S	3F	3F	3F
	0	1S	1S	2S	2S	3S	3F	3F	3N
10	0	0	0	0	0	0	0	0	*
	0	0	0	0	0	0	2S	2S	*
	0	0	0	0	0	0	0	0	*
60	0	0	0	0	0	0	0	0	*
	0	0	0	0	0	0	0	0	*
	0	0	0	0	0	0	0	0	0
270	0	0	0	0	0	0	0	0	0
	0	0	0	0	0	0	0	*	*
18 hours	0	0	0	0	0	0	*	*	*
	1SE	2FE	2FE	2FE	2NE	3NE	-	-	-

*… material broke near the clamp mounting point

The aforementioned epoxidation reactions resulted in a smaller positive effect on the ozone resistance of elastomers (Table 27), when applied on material C. Moreover, when applying a reaction time of 60- and 270-minutes the surface showed major cracks even before the static strain test was started, due to surface brittleness.

Table 27: static strain test data epoxidation B of material C; 10 % strain, 96 hours conditioning at rt, 50 pphm ozone, 55 % RH, 40 °C

reaction time in min	crack assessment time in hours								
	1	**2**	**3**	**5**	**9**	**25**	**49**	**73**	**97**
blank	1N	1N	1N	2N	2N	3N	3N	3N	3N
1	0	0	2S	2S	2S	3S	3S	3S	3S
10	0	1SE	2SE	2SE	2FE	2F	3F	3F	3F
18 hours	1S	2N	2N	3N	3N	3N	-	-	-

6 Conclusion and outlook

Concerning the possible formation of a pre-passivation layer – deriving from a surface reaction of ozone with rubber in the unstretched condition – and its positive impact on the ozone resistance of rubber, no significant respectively reproducible effect could be reported in this thesis against earlier observations and literature claims (*c.f.* 3.5.2.1). Several different ozone concentrations and reaction times were evaluated, but the possible negative effects like chain scission and increasing surface roughness – due to the ozone attack – seemed to dominate the pre-passivation trials.

To achieve an improved ozone stability of rubber, different other surface modifications were developed and tested. However, a catalyzed surface oxidation and a dihydroxylation with $KMnO_4$ proved to have no positive impact on the ozone resistance of rubber. On the other hand, surface chlorination reactions with acidified aqueous NaOCl solution and short reaction times showed an improvement concerning the crack free period with a factor of 3-9 compared to the blank. In addition, mild surface epoxidation reactions with m-CPBA proved to be the best choice, regarding the improvement of the ozone resistance of rubber. This surface modification results in at least 25 times longer crack free periods compared to an unmodified blank. Especially when longer reaction times (>10 min) were applied the positive impact on the ozone resistance was accompanied with an embrittlement of the rubber material and therefore affecting its crucial elastic properties.

Furthermore, selected surface modifications were characterized with ATR/FT-IR, XPS and SFE measurements.

In future studies the chlorination reaction and the epoxidation reaction should be investigated in detail and boundary conditions – like temperature, concentration and reaction time – should be optimized. Additionally, when looking at the epoxidation reaction, a variation of the solvent may result in improvements regarding the impairment of bulk properties like elasticity. This may be due to a change in the penetration depth of the solvent and in the course of this optimization, epoxidation of deeper rubber layers, may be prevented. The optimum of these parameters should be easily found when using a DOE approach.

Finally, the aforementioned surface modifications should be tested and optimized at different elastomeric materials. Also, higher saturated rubbers and blends (e.g. EPDM) may benefit from such modifications, yet not with the same huge impact as earlier described. In further steps the mechanical properties of the modified elastomers should be evaluated.

Nevertheless, covalent surface modifications on polymeric chains of rubber may hold good abrasion resistance, due to the fact that the macromolecules extend into the bulk.

With the help of a DOE approach, it could be illustrated that the degradation rate of rubber – due to the attack of ozone – seems not only to be depending on the number of surface double bonds (*cf.* 3.4), but also on its morphological structure and the surface to bulk ratio. These findings were discovered during the evaluation of production parameters – differing between

hydraulic hoses and laboratory test specimens – with a possible adverse effect on the ozone resistance of rubber.

The gathered information may be transferred to the hydraulic hose production, in the future. It is likely that this task will be achieved by using a non-structured tape in order to prevent a three-dimensional imprint on the hose's surface. A detailed investigation of the cost-value ratio, technical feasibility and market acceptance have to be successfully completed in advance.

In addition, the aforementioned and at some point, optimized chemical surface modifications may be used to prolong material failure – due to ozone degradation – of hydraulic hoses with a structured surface. A combination of an improved surface structure and the application of such chemical surface modifications may result in highly ozone resistant rubber hoses. Such long lasting hydraulic hoses are not only needed in applications with high ozone background concentrations, but also when small bending radii are needed – e.g. when the installation space is limited, due to compact and lightweight hydraulic equipment.

7 Experimental part

7.1 Rubber sheet production in laboratory scale

The raw materials (overall weight for each batch approx. 1.4-1.8 kg) were weight in according to the exact rubber recipe (which will not be displayed in this thesis due to IP issues) and mixed with an internal mixer (GK 1,5 E; Krupp Elastomertechnik; the mixing pattern is shown in Table 28). The temperature of the internal mixer was preset to 50 °C and during the entire mixing time of 300 seconds the temperature of the mixture was not allowed to exceed 165 °C. In order to assure this limit, the rotor speed was reduced as soon as temperature of 155 °C was reached. After the drop out of the rubber batch, its internal temperature was measured. The raw rubber was then processed on an open mill ("Comerio Ercole SPA") – for further homogenization and cooling (five repetitions) – to a rough sheet of about 6-7 mm thickness. After a resting time of 24 hours the vulcanization system, which was weight in separately, was added on an open mill. Again, the rubber sheet had to rest for 24 hours before the raw rubber was milled to appropriate thickness and cut into the dimensions fitting the press mold, to be then vulcanized in a hydraulic press at a pressure of 320 bars. The size of the final rubber sheets therefore was 300 x 300 x 0.8/2 mm respectively 200 x 200 x 0.8/2 mm for the part of the production parameter investigations and 300 x 300x 2 mm for the surface modification experiments. The vulcanization time and temperature are shown in Table 29 and are depending on the material (due to individual curing characteristics) and the experiment.

Table 28: mixing program internal mixer

time in sec	step
0	polymer addition (open ram)
10	ram down
60	ram up; addition of filler, softener, anti-ageing agents, processing aids
75	ram down
180	ram up: cleaning step
190	ram down
300	end of mixing, drop out of raw rubber batch

Table 29: vulcanization parameters

experiment	material	vulcanization time in min	vulcanization temperature in °C
production parameters	A	120	137
		60	150
surface modifications	B	30	150
	C	60	150

All used rubber materials are carbon black filled and sulfur crosslinked. The following polymers were used: EPDM and SBR in material A; SBR, BR and NR in material B; BR and NR in material C. In all formulations no antiozonants or paraffinic waxes were present.

7.2 Static strain test

The ozone resistance of the rubber was quantified by a static strain test and carried out according to the standard ISO 1431-1:2012. For the detailed crack assessment, the two-parameters-scale, which is proposed in appendix C (see Table 31), of the earlier mentioned standard, was used. Certainly, being aware of the disadvantages – also quoted in this appendix – that are associated with such a detailed crack assessment.

The ozone chamber ("Argentox, Ozone Technology Germany") was held at a constant temperature of 40 °C, a relative humidity of 55 % and an ozone concentration of 50 pphm. After the specimens (100 x 12 mm) were stamped out of the rubber sheets they were pre-conditioned at room temperature with applied strain, which varied between the materials, for 96 hours. It has to be added that the strain was applied in the same direction of the last milling step, since the preferred direction of the macromolecules is the same. The crack assessment was conducted after defined periods of time for different total exposition times, depending on the experiment and the material, stated in the following table (Table 30).

Table 30: crack assessment parameters

experiment	material	applied strain in %	crack assessment in hours	total exposition time in h
production parameters	A	30	every 4	120
surface modifications	B C	10	1, 2, 3, 5, 9, 25*	25*

*If no crack could be reported after 25 hours, the cracks were further evaluated in a 24-hour interval.

Table 31: crack assessment legend according to ISO 1431-1:2012

	crack dimensions		crack density
0	no cracks	S	hardly any cracks
1	cracks only visible with magnifier	F	relatively few cracks
2	no magnifier needed; cracks smaller than 0.5 mm	N	worse
3	worse		

If the cracks are only visible on the edges of the static strain test specimen, a "E" is added to the crack assessment code.

7.3 Production parameters

For roughness measurements of the different nylon tapes, a microscope ("Keyence, VHX-6000") was used with a magnification of 100x. The roughness was determined with the help of the software ("VHX-6000©, Version 3.0.0.115, Keyence corporation") and each tape was measured at three different locations.

The DOE was planned and evaluated with the JMP software ("JMP® 13.2.1, SAS Institute Inc.").

According to the DOE plan (Table 6) the different rubber sheets (300x300x2/0.8 mm or 200x200x2/0.8 mm) were produced as depicted in 7.1. For sheets with a nylon tape imprint the

nylon tape was placed in an angle of 45° to the preferred direction of the macromolecules – which were aligned due to the last milling step – between the rubber sheet and the metal cover of the press mold. If the DOE plan suggested an overlap, the tape was stacked to 50 % (*c.f.* Figure 25 and Figure 26). During the preparation of the test specimens, through stamping out, it was ensured that the overlap with its deepening was placed in the middle of the specimen for an ideal crack assessment. Moreover, beside the standard 2 mm mold, also 0.8 mm molds were used in accordance with the DOE plan. After vulcanization and 24 hours resting time the tape was carefully removed.

7.4 Surface modification

7.4.1 Ozone pre-passivation

The ozone test specimens were exposed to ozone in an ozone chamber ("Argentox, Ozone Technology Germany") at unstrained condition. The time between the launch and shutdown of the chamber was recorded. Since the buildup of a defined ozone concentration after starting the chamber and the decomposition of the ozone after the shutdown approximately need the same amount of time, the indicated exposition time describes nearly the true exposition time. In order to passivate the complete surface of the material, the specimens were exposed in a hanging condition. The pre-passivation tests were mainly conducted at a chamber temperature of 30 °C and a relative humidity of 55 %. The following table (Table 32) shows the different applied ozone concentration and the reaction times.

Table 32: ozone pre-passivation; reaction time and ozone concentration

ozone concentration in pphm	reaction time in hours								
10	0.17	0.5	1	2	4	7	-	-	-
50	0.17	0.5	1	2	4	7	24*	96*	168*
200	1**	2**	4**	8**	24	96	-	-	-

*These conditions were tested with a temperature of 40 °C instead of 30 °C
**These conditions were also tested with 80 % RH

The modified specimens were subjected to the static strain test or surface characterizations were performed after a resting time of 24 hours.

7.4.2 Catalyzed oxidation

A 500 mL long shaped beaker was charged with 300 mL ethanol and $CuCl_2$ (75.0 g, 558 mmol). The rubber specimens were added under continuous stirring to the homogeneous solution at room temperature. After 30 seconds, 60 seconds and 1 hour the specimens were removed and left to dry overnight. Subsequently the samples were exposed to UV-light (Xenon lamp 300-400 nm, Original Hanau Suntest) for 0-, 2-, 6- and 24-hours. Over the course of this photooxidation the green $CuCl_2$ precipitate on the rubber surface turned brownish. The specimens were rinsed with water and dried with paper towels. Then they were subjected to

the static strain test and in parallel surface characterizations were performed after a resting time of 24 hours.

7.4.3 Dihydroxylation

A 500 mL long shaped beaker was charged with 300 mL water and $KMnO_4$ (47.4 g, 300 mmol). After the oxidizing agent was completely dissolved at room temperature the pH-value of the solution was adjusted with solid NaOH to a value of approx. 9. The rubber specimens were added under continuous stirring (room temperature and 5 °C). After the reaction time (1 min, 10 min, 60 min) was elapsed the specimens were rinsed with water and dried with paper towels. The modified specimens were subjected to the static strain test and in parallel surface characterizations were performed after a resting time of 24 hours.

7.4.4 Chlorination

A 500 mL long shaped beaker was charged with 300 mL aqueous NaOCl solution (approx. 13 %) of technical grade and it was acidified (pH ≈ 4) with aqueous HCl solution (30 %), whereupon gas evolution was observed. At room temperature the rubber specimens were added under continuous stirring. After the reaction time (1 min, 10 min, 60 min) was elapsed the specimens were rinsed with water and dried with paper towels. The modified specimens were subjected to the static strain test and in parallel surface characterizations were performed after a resting time of 24 hours.

7.4.5 Epoxidation

7.4.5.1 Approach A (NaOCl/KBr)

A 500 mL long shaped beaker was charged with 300 mL aqueous NaOCl solution (approx. 13 %) of technical grade and KBr (93.5 g, 786 mmol, 1.5 equiv. based on NaOCl). At room temperature the rubber specimens were added under continuous stirring to the orange solution. After the reaction time (1 min, 10 min, 60 min, 120 min) was elapsed, the specimens were rinsed with water and dried with paper towels. The modified specimens were subjected to the static strain test and in parallel surface characterizations were performed after a resting time of 24 hours.
This surface epoxidation was conducted according to a modified literature protocol.[44]

7.4.5.2 Approach B (m-CPBA)

A 500 mL long shaped beaker was charged with m-CPBA (30.0 g, 174 mmol) and 300 mL 2-propanole. After the oxidizing agent was completely dissolved at room temperature, the rubber specimens were added under continuous stirring to the solution. After the reaction time (1 min, 10 min, 60 min, 270 min, 18 hours) was elapsed the specimens were rinsed with ethanol and

dried with paper towels. The modified specimens were subjected to the static strain ozone test and in parallel surface characterizations were performed after a resting time of 24 hours. This surface epoxidation was conducted according to a modified literature protocol.[45]

7.5   Surface characterization

7.5.1   ATR/FT-IR

For the ATR/FT-IR characterization, following a background scan, the sample was placed on the ATR element ("PIKE, MIRacle™") containing a Germanium crystal. Pressure was applied with the high-pressure clamp, using its slip-clutch mechanism. The spectra were measured with the FT-IR spectrometer ("Bruker Optik GmbH, Tensor 27") and further processed with OPUS© (Version 4.2, Bruker Optik GmbH) software. The ATR-crystal was cleaned with ethanol between each sample.

7.5.2   SFE

The contact angles of water and diiodomethane, building up in contact with the modified rubber surface, were measured on a "Krüss DSA30". Two exemplary measurements of the contact angles of samples with a high and a low SFE are shown in the Appendix (*c.f.* Figure 16 and following). Therefore, the specimen was placed on the sample table and after the focus of the camera ("Allied Vision Technologies Stingray") was optimized, the software ("Krüss Advance 1.5.1.0") was calibrated with the dimensions of the earlier measured dispensing needle. In the next step the drop was dispensed (approx. 4 µL), and the contact angle and the real volume (with the help of the liquids density and the outer dimensions) of the drop were determined by the software. Each drop was measured six times and each solid-liquid pair was repeated 8 times. The SFE was then calculated by the software with the Owens, Wendt, Rabel and Kaelble (OWRK) method.

7.5.3   XPS

XPS measurements were performed at the TU Wiens Analytical Instrumentation Center (AIC) by Dr. Annette Foelske and Dr. Markus Sauer as following:
"All measurements were carried out a SPECS XPS-spectrometer equipped with a monochromatised Al-Kα X- ray source (µFocus 350) and a hemispherical WAL-150 analyser (acceptance angle: 60°).
Pass energies of 100 eV and 30 eV and energy resolutions of 1 eV and 100 meV were used for survey and detail spectra respectively (Excitation energy: 1486.6 eV, Beam energy and spot size: 70 W onto 500 µm; Mean angle: 51° to sample surface normal; Base pressure: 1×10^{-9} mbar, Pressure during measurements: 3×10^{-9} mbar).
Ar-ion sputtering was carried out with a SPECS IQ 38/11 ion gun using 3 kV acceleration voltage and 2×10^{-7} mbar Ar partial pressure, creating a beam that is rastered over a $2\times2mm^2$ spot on the sample.

Data analysis was performed using CASA XPS software, employing transmission corrections (as per the instrument vendor's specifications), Shirley/Tougaard backgrounds [D.A. Shirley, Phys. Rev. B 5, 4709 (1972) / S. Tougaard, Surf. Interf. Anal. 25, 137 (1997)] and Scofield sensitivity factors [J. H. Scofield, J. Electron. Spectroscop. Relat Phenom. 8, 129 (1976)]. Charge correction was applied so the adventitious carbon peak (C-C peak) was shifted to approximately 285 eV binding energy (BE).

All content values shown are in units of relative atomic percent (at%), where the detection limit in survey measurements usually lies around 0.1-0.5 at%, depending on the element. Assignment of different components was primarily done using Refs. [C.D. Wagner, A.V. Naumkin, A. Kraut-Vass, J.W. Allison, C.J. Powell, J.R. Rumble, NIST Standard Reference Database 20, Version 3.4 (web version) (http:/srdata.nist.gov/xps/) 2003; G. Beamson, D. Briggs, High Resolution XPS of Organic Polymers - The Scienta ESCA300 Database, Wiley, 1992, Appendices 3.1 and 3.2.]."[58]

He who, in the strict sense, lives only for science, is an idolater; how often do I thus err and how many others are guilty without recognizing the horror and culpability of this sin.[1]

Christian Friedrich Schönbein

8 List of abbreviations

AICc	Akaike information criterion correction
ATR/FT-IR	attenuated total reflection Fourier transform infrared spectroscopy
BE	binding energy
BIC	Bayesian information criterion
BR	butadiene rubber
CA	contact angle
DOE	design of experiments
DPPD	N,N'-Diphenyl-p-phenylenediamine
DTDM	dithiodimorpholine
EPDM	ethylene propylene diene monomer
E-SBR	emulsion styrene butadiene rubber
IPCC	Intergovernmental Panel on Climate Change
IPPD	N-Isopropyl-N′-phenyl-1,4-phenylenediamine
LOP	lipid ozonation product
m-CPBA	meta-chloroperbenzoic acid
NBR	nitrile butadiene rubber
NR	natural rubber
PAF	platelet-activating factor
PLA_2	Phospholipase A_2
$PM_{2,5}$	particulate matter 2.5 µm
POP-Oz	l-palmitoyl-2-oleoyl-sn-glycerol-3-phosphocholine ozonide
PP	polypropylene
ppb	parts per billion
PPDA	p-phenylene diamine
6-PPD	N-(1,3-dimethylbutyl)-N'-phenyl-1,4-benzenediamine
pphm	parts per hundred million
PVC	polyvinyl chloride
RH	relative humidity
Sa	arithmetical mean height
SBR	styrene butadiene rubber
SFE	surface free energy
Sp	maximum peak height
Sq	root mean square height
S-SBR	solution styrene butadiene rubber
Sv	maximum pit height
Sz	maximum height
TCICA	trichloroisocyanuric acid
TMTD	tetramethylthiuram disulfide
UHV	ultrahigh vacuum
UV	ultraviolet
XPS	X-ray photoelectron spectroscopy

9 References

1. Oesper, R. E., Christian Friedrich Schonbein. Part I. Life and character. *Journal of Chemical Education* **1929,** *6*, 432.
2. Greve, H.-H.; Threadingham, D., Rubber, 1. Survey. In *Ullmann's Encyclopedia of Industrial Chemistry*.
3. Engels, H.-W.; Weidenhaupt, H.-J.; Pieroth, M.; Hofmann, W.; Menting, K.-H.; Mergenhagen, T.; Schmoll, R.; Uhrlandt, S., Rubber, 9. Chemicals and Additives. In *Ullmann's Encyclopedia of Industrial Chemistry*,2011.
4. Greve, H.-H., Rubber, 2. Natural. In *Ullmann's Encyclopedia of Industrial Chemistry*.
5. Brandt, H.-D.; Nentwig, W.; Rooney, N.; LaFlair, R. T.; Wolf, U. U.; Duffy, J.; Puskas, J. E.; Kaszas, G.; Drewitt, M.; Glander, S., Rubber, 5. Solution Rubbers. In *Ullmann's Encyclopedia of Industrial Chemistry*.
6. Obrecht, W.; Lambert, J.-P.; Happ, M.; Oppenheimer-Stix, C.; Dunn, J.; Krüger, R., Rubber, 4. Emulsion Rubbers. In *Ullmann's Encyclopedia of Industrial Chemistry*.
7. Röthemeyer, F.; Sommer, F., Kautschuk Technologie. 3 ed.; Hanser Verlag2013; pp 1166-1173.
8. Bailey, P. S., CHAPTER I - Introduction. In *Ozonation in Organic Chemistry*, Bailey, P. S., Ed. Academic Press1978; pp 1-5.
9. Rubin, M. B., The History of Ozone. The Schönbein Period, 1839-1868. *Bull. Hist. Chem.* **2001,** *26*, 40-56.
10. Rubin, M. B., The History of Ozone. Part III. *Helvetica Chimica Acta* **2003,** *86*, 930-940.
11. Bailey, P. S., CHAPTER II - The Ozone Molecule. In *Ozonation in Organic Chemistry*, Bailey, P. S., Ed. Academic Press1978; pp 7-8.
12. Bailey, P. S., CHAPTER I - Introduction. In *Ozonation in Organic Chemistry*, Bailey, P. S., Ed. Academic Press1982; pp 1-2.
13. Bailey, P. S., CHAPTER IV - Ozonolysis of Olefins: Initial Ozone Attack and Adduct. In *Ozonation in Organic Chemistry*, Bailey, P. S., Ed. Academic Press1978; pp 15-24.
14. Bruice, P. Y., The addition of ozone to an alkene: ozonolysis. In *Organic Chemistry*, 8 ed.; Pearson2016.
15. Bailey, P. S., CHAPTER IX - Ozone Attack at sp3 Carbon Centers: Ozonation of Carbon–Hydrogen Bonds. In *Ozonation in Organic Chemistry*, Bailey, P. S., Ed. Academic Press1982; pp 255-328.
16. Bailey, P. S., CHAPTER III - Ozonation of Aromatic Compounds: Benzene and Substituted Benzenes. In *Ozonation in Organic Chemistry*, Bailey, P. S., Ed. Academic Press1982; pp 18-42.
17. Bailey, P. S., CHAPTER VII - Ozonation of Nucleophiles. In *Ozonation in Organic Chemistry*, Bailey, P. S., Ed. Academic Press1982; pp 155-224.
18. Pryor, W. A.; Squadrito, G. L.; Friedman, M., The cascade mechanism to explain ozone toxicity: The role of lipid ozonation products. *Free Radical Biology and Medicine* **1995,** *19*, 935-941.
19. Jerrett, M.; Burnett, R. T.; Pope, C. A.; Ito, K.; Thurston, G.; Krewski, D.; Shi, Y.; Calle, E.; Thun, M., Long-Term Ozone Exposure and Mortality. *New England Journal of Medicine* **2009,** *360*, 1085-1095.
20. Vingarzan, R., A review of surface ozone background levels and trends. *Atmospheric Environment* **2004,** *38*, 3431-3442.
21. Allen, N. S.; Edge, M.; Mourelatou, D.; Wilkinson, A.; Liauw, C. M.; Dolores Parellada, M.; Barrio, J. A.; Ruiz Santa Quiteria, V., Influence of ozone on styrene–

ethylene–butylene–styrene (SEBS) copolymer. *Polymer Degradation and Stability* **2003,** *79*, 297-307.

22. Abts, G., Einführung in die Kautschuktechnologie. **2018**, 63.

23. Salomon, G.; Van Bloois, F., The mechanism of ozone cracking. I. Ozone cracking of plastic films. *Journal of Applied Polymer Science* **1963,** *7*, 1117-1132.

24. Cataldo, F., On the ozone protection of polymers having non-conjugated unsaturation. *Polymer Degradation and Stability* **2001,** *72*, 287-296.

25. Giurginca, M.; Zaharescu, T.; Meghea, A., Degradation of ethylene-propylene elastomers in the presence of ozone. *Polymer Degradation and Stability* **1995,** *50*, 45-48.

26. Tucker, H., The Reaction of Ozone with Rubber. *Rubber Chemistry and Technology* **1959,** *32*, 269-277.

27. PIETERS, E. Verfahren zur Modifizierung der Oberfläche eines Wischblatts für Scheibenwischer unter Einwirkung von Ozon. 2010.

28. Danielle Galiani, P.; Antonio Malmonge, J.; Guenther Soares, B.; Henrique Capparelli Mattoso, L., Studies on thermal–oxidative degradation behaviours of raw natural rubber: PRI and thermogravimetry analysis. *Plastics, Rubber and Composites* **2013,** *42*, 334-339.

29. Kuzminskii, A. S.; Degteva, T. G.; Lapteva, K. A., The Mechanism of Oxidation of Synthetic Rubbers. *Rubber Chemistry and Technology* **1956,** *29*, 573-582.

30. Cadek, D. r.; Zvolská, K. i.; Kadeřábková, A.; Hrdlička, Z. k.; Havlín, J., The Role of Copper Compounds as Thermooxidation Catalysts. *KGK Rubberpoint* 2020.

31. Hong Goh, S.; Wah Phang, K., Thermoanalytical studies of rubber oxidation catalyzed by metallic ions. *Thermochimica Acta* **1978,** *25*, 109-115.

32. Buizov, B. V.; Molodenskii, V. S.; Mikhailov, N. I., The Action of Copper Salts on Raw Rubber. *Rubber Chemistry and Technology* **1934,** *7*, 618-631.

33. Williams, I., Oxidation of Rubber Exposed to Light. *Industrial & Engineering Chemistry* **1926,** *18*, 367-369.

34. Taylor, J. E.; Williams, D.; Edwards, K.; Otonnaa, D.; Samanich, D., Permanganate peroxidation of cyclohexene.I. The unusual effect of turbulent stirring and dilution upon glycol yields. *Canadian Journal of Chemistry* **1984,** *62*, 11-15.

35. Wiberg, K. B.; Saegebarth, K. A., The Mechanisms of Permanganate Oxidation. IV. Hydroxylation of Olefins and Related Reactions. *Journal of the American Chemical Society* **1957,** *79*, 2822-2824.

36. Taylor, J. E.; Green, R., Permanganate peroxidation of cyclohexene. III. Hydroxide ion and salt effect studies. *Canadian Journal of Chemistry* **1985,** *63*, 2777-2780.

37. Martin-Martinez, J. M.; Fernandez-Garcia, J. C.; Huerta, F.; Orgiles-Barcelo, A. C., Effect of Different Surface Modifications on the Adhesion of Vulcanized Styrene-Butadiene Rubber. *Rubber Chemistry and Technology* **1991,** *64*, 510-521.

38. Bruice, P. Y., The addition of a halogen to an alkene. In *Organic Chemistry*, 8 ed.; Pearson2016.

39. Waddell, W. H.; Evans, L. R.; Gillick, J. G.; Shuttleworth, D., Polymer Surface Modification. *Rubber Chemistry and Technology* **1992,** *65*, 687-696.

40. Lawson, D. F.; Kim, K. J.; Fritz, T. L., Chemical Modifications of Rubber Surfaces: XPS Survey of the Reactions of Trichloroisocyanuric Acid at the Surfaces of Vulcanized Elastomers. *Rubber Chemistry and Technology* **1996,** *69*, 245-252.

41. Abraham, E. K.; Ramesh, P., NATURAL RUBBER LATEX PRODUCTS: CONCERNS IN HEALTH CARE. *Journal of Macromolecular Science, Part C* **2002,** *42*, 185-234.

42. Katsuki, T.; Sharpless, K. B., The first practical method for asymmetric epoxidation. *Journal of the American Chemical Society* **1980,** *102*, 5974-5976.

43. Liu, G. Y. T.; Richey, W. F.; Betso, J. E.; Hughes, B.; Klapacz, J.; Lindner, J., Chlorohydrins. In *Ullmann's Encyclopedia of Industrial Chemistry*; pp 1-25.

44. Klawonn, M.; Bhor, S.; Mehltretter, G.; Döbler, C.; Fischer, C.; Beller, M., A Simple and Convenient Method for Epoxidation of Olefins without Metal Catalysts. *Advanced Synthesis & Catalysis* **2003,** *345*, 389-392.

45. Roland, C. M.; Zemel, I.; Chester F. Poranski, J. Surface epoxidation of elastomers. 1994.

46. Martinez, L.; Roman, E.; Nevshupa, R., X-Ray Photoelectron Spectroscopy for Characterization of Engineered Elastomer Surfaces. In *Advanced Aspects of Spectroscopy*, Farrukh, M. A., Ed. IntechOpen2012.

47. Sanches, N. B.; Pedro, R.; Diniz, M. F.; Mattos, E. d. C.; Cassu, S. N.; Dutra, R. d. C. L., Infrared Spectroscopy Applied to Materials Used as Thermal Insulation and Coatings. *Journal of Aerospace Technology and Management* **2013,** *5*, 421-430.

48. PIKE_Technologies Analysis of Polymers by ATR/FT-IR Spectroscopy. https://www.piketech.com/files/pdfs/Analysis_of_Polymers_ATR_FTIR_AN.pdf (01.12.2020),

49. Gregoriou, V. G., FOURIER TRANSFORM INFRARED SPECTROSCOPY OF POLYMERS. In *Applied Polymer Science: 21st Century*, Craver, C. D.; Carraher, C. E., Eds. Pergamon: Oxford, 2000; pp 709-757.

50. CR_KrüssGmbH Models for Surface Free Energy Calculation. https://www.kruss-scientific.com/fileadmin/user_upload/website/literature/kruss-tn306-en.pdf (01.12.2020),

51. Zenkiewicz, M., Methods for the calculation of surface free energy of solids. *Journal of Achievements in Materials and Manufacturing Engineering* **2007,** *24*.

52. Ebnesajjad, S., Surface Tension and Its Measurement. *Handbook of Adhesives and Surface Preparation* **2011**, 21-30.

53. Oswald, S., X-Ray Photoelectron Spectroscopy in Analysis of Surfaces Update based on the original article by Steffen Oswald, Encyclopedia of Analytical Chemistry, © 2000, John Wiley & Sons, Ltd. In *Encyclopedia of Analytical Chemistry*.

54. Romero-Sanchez, M. D.; Mercedes Pastor-Blas, M.; Martín-Martínez, J. M.; Walzak, M. J., Addition of ozone in the UV radiation treatment of a synthetic styrene-butadiene-styrene (SBS) rubber. *International Journal of Adhesion and Adhesives* **2005,** *25*, 358-370.

55. Murakami, T. N.; Fukushima, Y.; Hirano, Y.; Tokuoka, Y.; Takahashi, M.; Kawashima, N., Surface modification of polystyrene and poly(methyl methacrylate) by active oxygen treatment. *Colloids and Surfaces B: Biointerfaces* **2003,** *29*, 171-179.

56. Pastor-Blas, M. M.; Sanchez-Adsuar, M. S.; Martin-Martinez, J. M., Surface modification of synthetic vulcanized rubber. *Journal of Adhesion Science and Technology* **1994,** *8*, 1093-1114.

57. Pavia, D. L.; Lampman, G. M.; Kriz, G. S., *Introduction to Spectroscopy*. 3 ed.

58. Foelske, A.; Sauer, M. *Photoelectron spectroscopy of elastomers report*; Analytical Instrumentation Center E057-05, Technische Universität Wien, Getreidemarkt 9, A-1060 Vienna15.12.2020, 2020.

10 Appendix

Figure 16: contact angel measurement between for 2 hours pre-passivated (200 pphm, 30 °C, 55 % RH) rubber and water
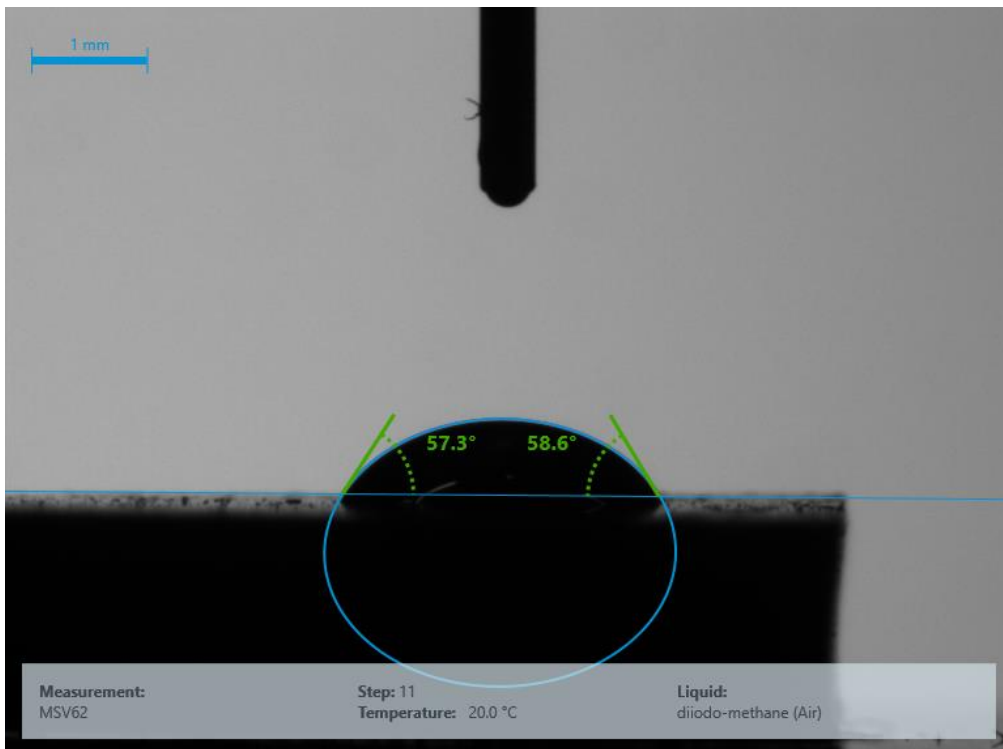

Figure 17: contact angel measurement between for 2 hours pre-passivated (200 pphm, 30 °C, 55 % RH) rubber and diiodomethane
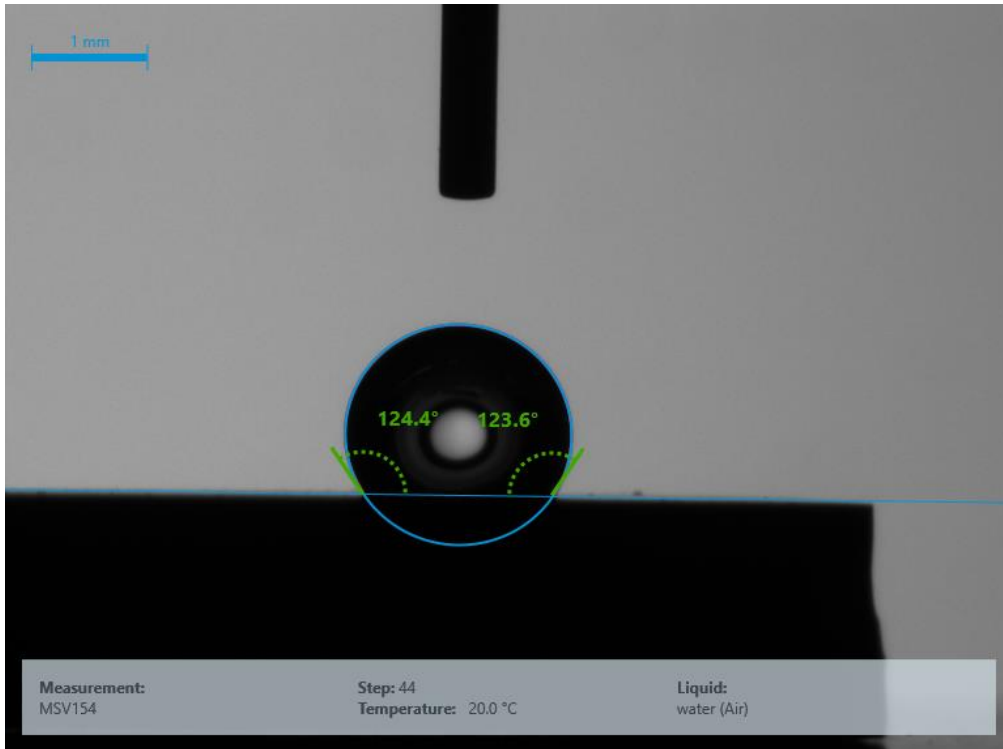
Figure 18: contact angel measurement between for 2 hours epoxidized rubber according to approach A and water
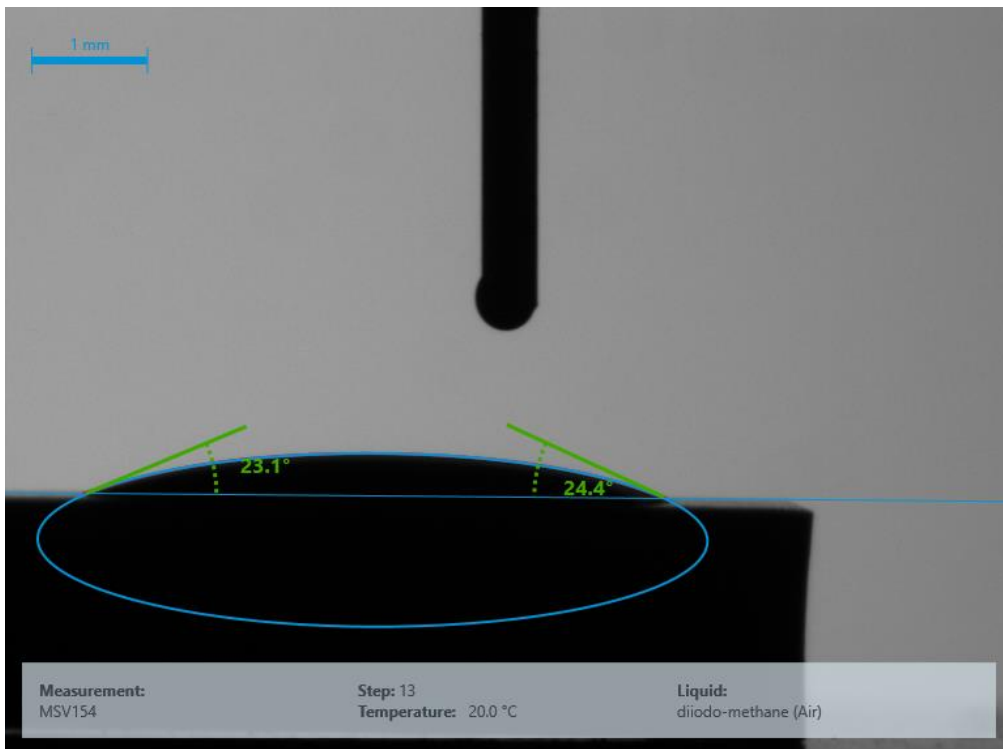
Figure 19: contact angel measurement between for 2 hours epoxidized rubber according to approach A and diiodomethane
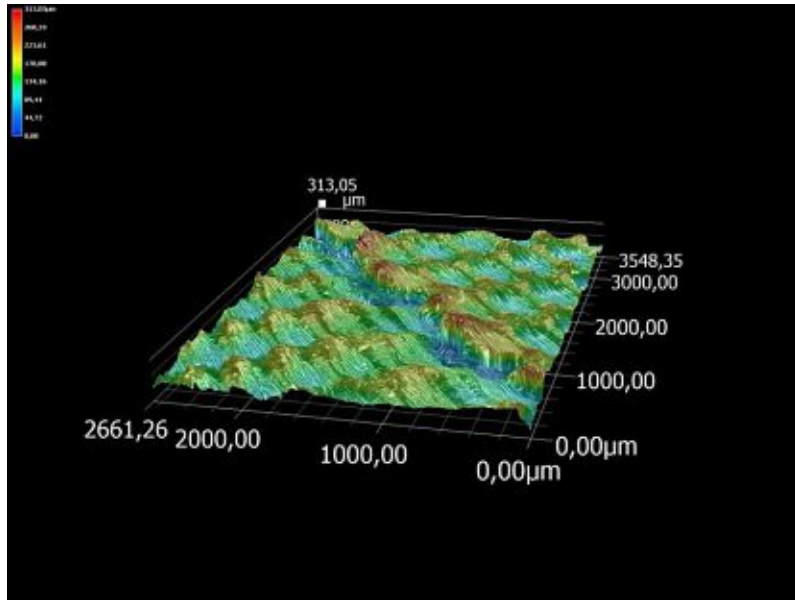
Figure 20: microscopic 3D picture (50x) of a hydraulic hose; tape overlap imprint clearly visible
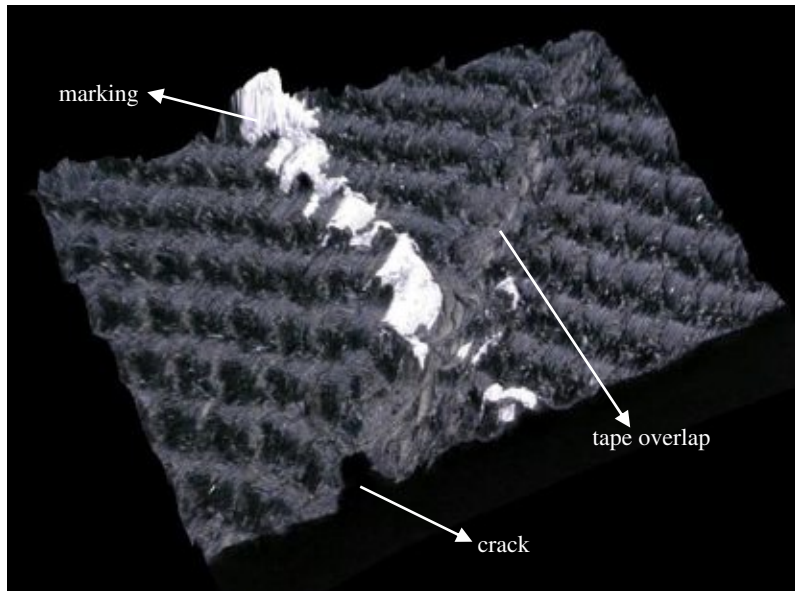
Figure 21: microscopic 3D picture (50x) of MS1P18 after 24 hours static ozone test; crack near the tape overlap imprint visible
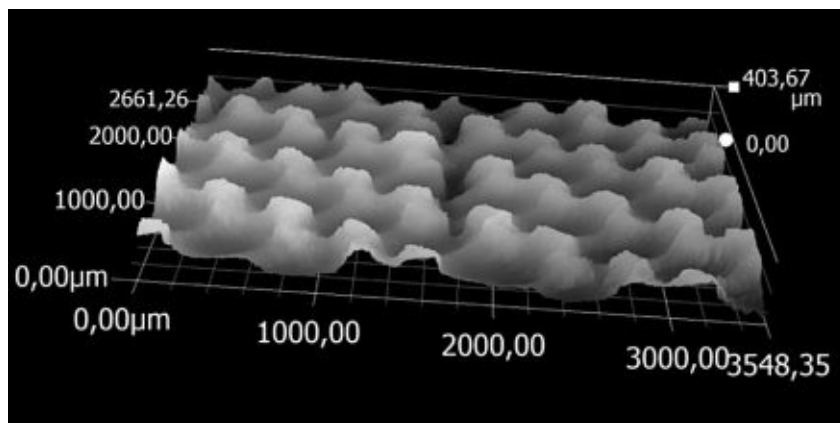
Figure 22: microscopic 3D picture (50x) of MS1P17 after 24 hours static ozone test; ozone crack in the middle of the picture visible
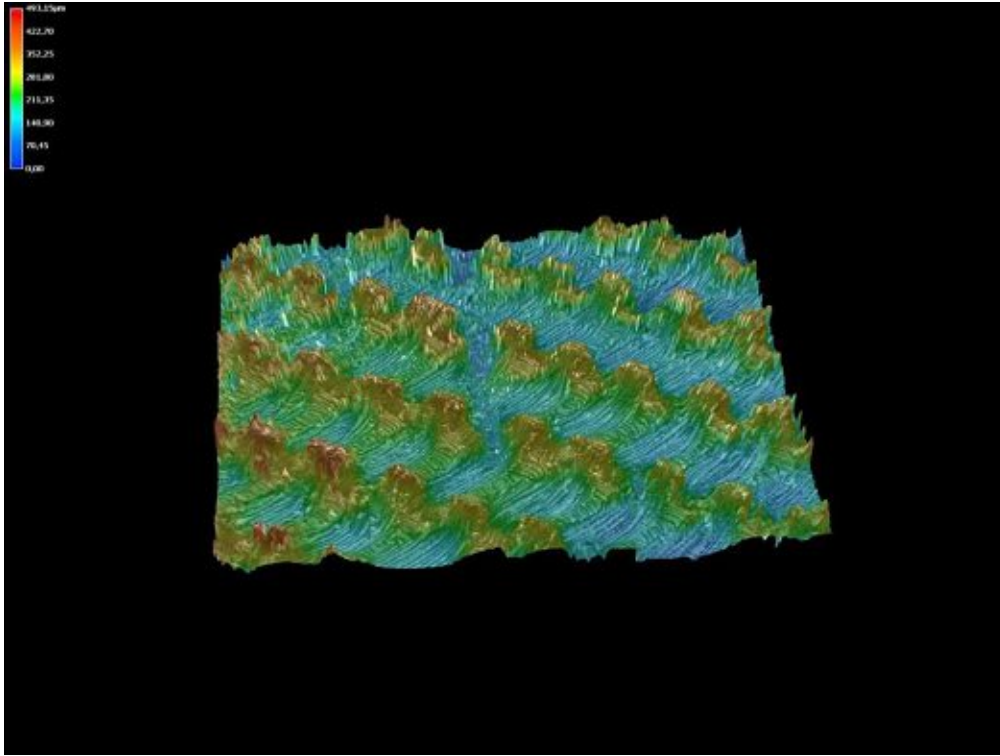
Figure 23: microscopic 3D picture (50x) of MS1P17 after 24 hours static ozone test; ozone crack in the middle of the picture visible
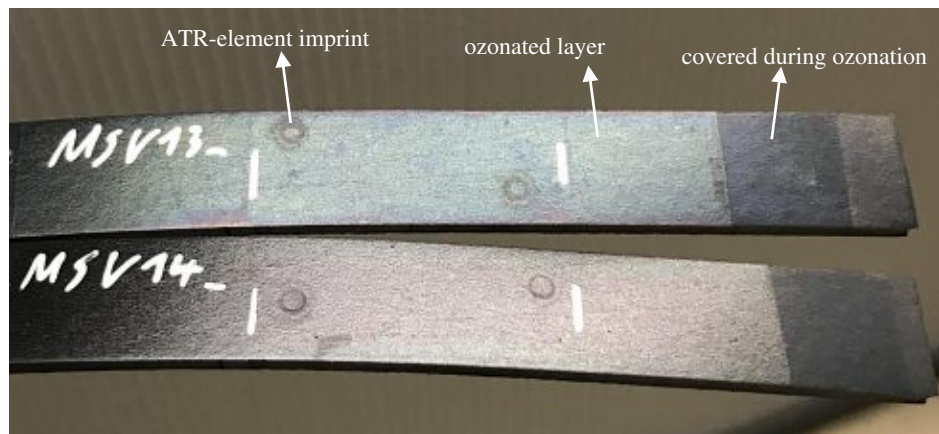
Figure 24: staining due to ozone pre-passivation 50 pphm, 40 °C, 55 % RH; top: 24 h, lowest: 96 h reaction time
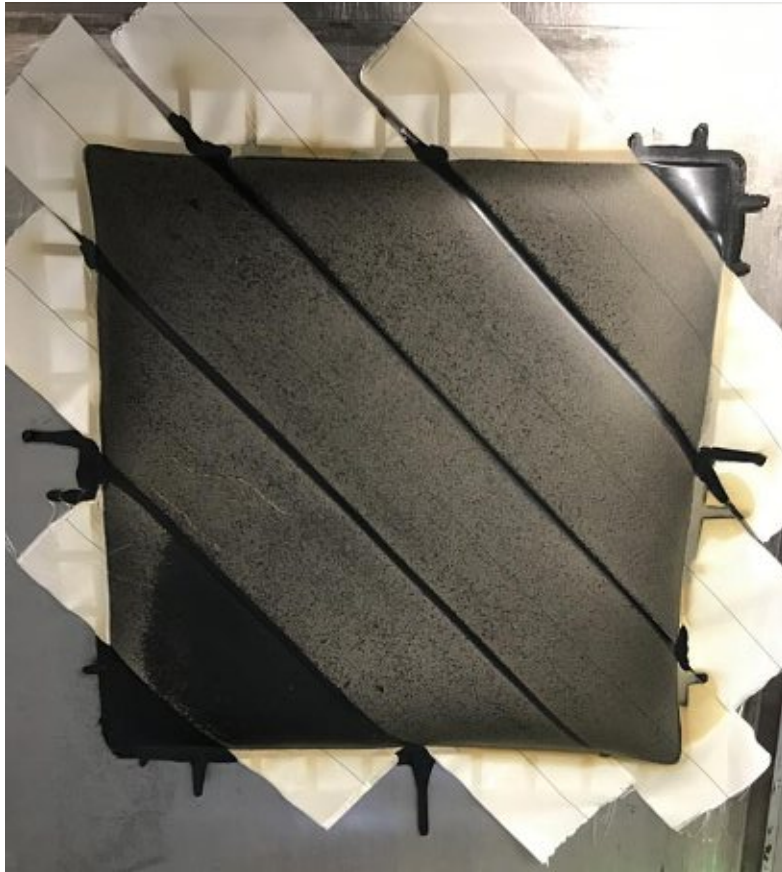
Figure 25: rubber sheet in production, process parameter evaluation; new tape without overlap
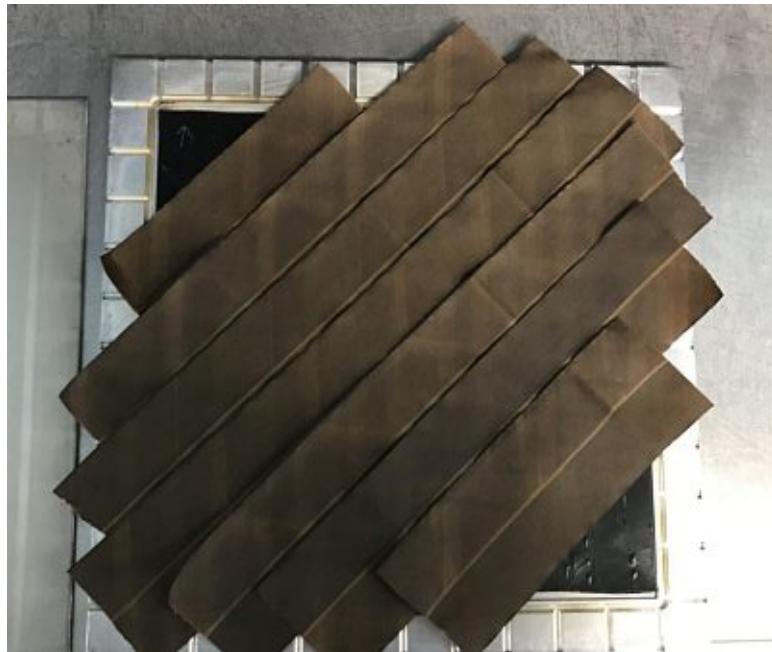
Figure 26: rubber sheet in production, process parameter evaluation; old tape with overlap

Table 33: extracted inflection points for both repetitions

rubber sheet	inflection point repetition 1 in h	inflection point repetition 2 in h	arithmetical mean in h
MSS1P1	59,93	38,28	49,11
MSS1P2	39,27	20,64	29,95
MSS1P3	36,36	38,61	37,49
MSS1P4	28,71	24,10	26,40
MSS1P5	39,27	40,77	40,02
MSS1P6	42,77	40,13	41,45
MSS1P7	44,73	84,87	64,80
MSS1P8	-	97,14	-
MSS1P9	54,25	62,03	58,14
MSS1P10	38,40	30,42	34,41
MSS1P11	64,86	61,91	63,39
MSS1P12	38,11	42,28	40,20
MSS1P13	4,69	23,89	14,29
MSS1P14	125,00	125,00	125,00
MSS1P15	46,90	-	-
MSS1P16	62,03	84,31	73,17
MSS1P17	23,80	31,17	27,48
MSS1P18	29,17	35,89	32,53
MSS1P19	23,28	24,66	23,97
MSS1P20	34,24	43,44	38,84
MSS1P21	57,17	80,38	68,77
MSS1P22	125,00	125,00	125,00
MSS1P23	97,14	125,00	111,07
MSS1P24	39,59	38,34	38,96
MSS1P25	31,61	37,04	34,33
MSS1P26	75,60	69,36	72,48
MSS1P27	36,12	39,46	37,79
MSS1P28	38,12	49,66	43,89
MSS1P29	12,69	46,05	29,37
MSS1P30	35,13	69,16	52,15

Table 34: production parameters evaluation, static strain test (30 % strain, 96 hours conditioning at rt, 50 pphm ozone, 55 % RH, 40 °C) data repetition 1

rubber sheet	ozone exposure time in hours																		
	4	8	12	16	20	24	28	32	36	40	44	48	52	56	60	68	72	96	120
MSS1P1	0	0	0	0	0	0	0	0	0	1SE	2SE	2SE	3SE	3SE	3SE	3S	3S	3F	3F
MSS1P2	0	0	0	0	0	0	0	0	0	2S	2S	-	-	-	-	-	-	-	-
MSS1P3	0	0	0	0	0	0	0	0	1S	1S	2S	2S	3S	3S	3F	3F	3F	3N	3N
MSS1P4	0	0	0	0	0	0	0	-	-	-	-	-	-	-	-	-	-	-	-
MSS1P5	0	0	0	0	0	0	0	0	0	2S	2S	-	-	-	-	-	-	-	-
MSS1P6	0	0	0	0	0	2SE	2SE	2SE	2SE	2SE	2S	3S	3S	-	-	-	-	-	-
MSS1P7	0	0	0	0	0	0	0	0	0	0	0	-	-	-	-	-	-	-	-
MSS1P8	0	0	0	0	0	0	0	0	0	0	0	0	0	2SE	3SE	3SE	3SE	3SE	3S
MSS1P9	0	0	0	0	0	0	0	0	0	0	0	2SE	2SE	3S	3S	3S	3S	3N	-
MSS1P10	0	0	0	0	0	0	0	1SE	1SE	2S	2S	3S	3S	3F	3F	3F	3F	3N	3N
MSS1P11	0	0	0	0	0	0	0	0	0	0	1SE	2SE	2SE	2SE	2SE	2SE	2S	3S	3S
MSS1P12	0	0	0	0	0	0	0	0	0	-	-	-	-	-	-	-	-	-	-
MSS1P13	0	-	-	-	-	-	-	-	-	-	-	-	-	-	-	-	-	-	-
MSS1P14	0	0	0	0	0	0	0	0	0	0	0	0	0	0	0	0	0	0	0
MSS1P15	0	0	0	0	0	0	0	0	0	1SE	2SE	-	-	-	-	-	-	-	-
MSS1P16	0	0	0	0	0	0	0	0	0	0	0	2SE	2SE	2SE	2SE	2S	2S	3S	3F
MSS1P17	0	0	0	0	0	2S	2S	2F	3F	3F	-	-	-	-	-	-	-	-	-
MSS1P18	0	0	0	0	2SE	2SE	2SE	-	-	-	-	-	-	-	-	-	-	-	-
MSS1P19	0	0	0	0	1SE	2S	2S	3F	-	-	-	-	-	-	-	-	-	-	-
MSS1P20	0	0	0	0	0	0	1SE	1SE	1S	2F	2F	3F	3F	3F	3F	3F	3F	3N	-
MSS1P21	0	0	0	0	0	0	0	0	0	0	0	0	0	1SE	2S	2S	2S	3S	3F
MSS1P22	0	0	0	0	0	2S	2S	2S	2S	2S	2S	2S	2S	2S	2S	2S	2S	2S	2S
MSS1P23	0	0	0	0	0	0	0	0	0	0	0	0	0	0	0	0	0	0	-
MSS1P24	0	0	0	0	0	0	0	0	0	1S	2S	3F	3F	3F	3F	-	-	-	-
MSS1P25	0	0	0	0	0	0	1SE	2S	2S	2S	3S	3S	3S	3S	3S	3F	3F	-	-
MSS1P26	0	0	0	0	0	0	0	0	0	0	0	1SE	2SE	2SE	2SE	2SE	3SE	3S	3S
MSS1P27	0	0	0	0	0	0	0	1SE	1S	2S	3S	3F	3F	3F	-	-	-	-	-
MSS1P28	0	0	0	0	0	0	0	0	0	1S	2S	2S	2S	3S	3F	3F	3F	3F	3F
MSS1P29	0	0	0	-	-	-	-	-	-	-	-	-	-	-	-	-	-	-	-
MSS1P30	0	0	0	0	0	0	0	1S	1S	2S	2S	3S	3S	3S	3S	-	-	-	-

"-" is indicating a total material failure

Table 35: production parameters evaluation, static strain test (30 % strain, 96 hours conditioning at rt, 50 pphm ozone, 55 % RH, 40 °C) data repetition 2

rubber sheet	ozone exposure time in hours																		
	4	8	12	16	20	24	28	32	36	40	44	48	52	56	60	68	72	96	120
MSS1P1	0	0	0	0	0	0	1SE	2SE	2SE	2S	2S	3F	3F	3F	3N	3N	3N	3N	-
MSS1P2	0	0	0	0	1S	1S	1S	-	-	-	-	-	-	-	-	-	-	-	-
MSS1P3	0	0	0	0	0	0	1SE	1SE	2SE	2S	2S	2F	3F	3F	3N	3N	3N	3N	-
MSS1P4	0	0	0	0	3SE	3SE	-	-	-	-	-	-	-	-	-	-	-	-	-
MSS1P5	0	0	0	0	0	0	0	0	0	0	-	-	-	-	-	-	-	-	-
MSS1P6	0	0	0	0	0	0	0	0	1SE	2SE	-	-	-	-	-	-	-	-	-
MSS1P7	0	0	0	0	0	0	0	0	0	0	0	0	0	0	0	0	0	-	-
MSS1P8	0	0	0	0	0	0	0	0	0	0	0	0	0	0	0	0	0	0	2S
MSS1P9	0	0	0	0	0	0	0	0	0	0	2SE	2SE	2SE	2SE	2SE	2S	2S	3S	3F
MSS1P10	0	0	0	0	0	0	1SE	1S	2S	2S	2F	2F	2F	2F	3F	3F	3F	3F	-
MSS1P11	0	0	0	0	0	0	0	0	0	0	0	1SE	2SE	2SE	2SE	2S	2S	2S	3F
MSS1P12	0	0	0	0	0	0	0	0	0	2SE	-	-	-	-	-	-	-	-	-
MSS1P13	0	0	0	0	1SE	2S	-	-	-	-	-	-	-	-	-	-	-	-	-
MSS1P14	0	0	0	0	0	0	0	0	0	0	0	0	0	0	0	0	0	0	0
MSS1P15	0	0	0	0	0	0	0	0	0	0	0	0	0	0	2SE	2SE	2SE	3SE	-
MSS1P16	0	0	0	0	0	0	0	0	0	0	1SE	1SE	1SE	1SE	1SE	1SE	2SE	2S	2S
MSS1P17	0	0	0	0	0	0	0	2S	3S	3F	3F	3F	3F	-	-	-	-	-	-
MSS1P18	0	0	0	0	0	0	0	2S	-	-	-	-	-	-	-	-	-	-	-
MSS1P19	0	0	0	0	0	2S	2S	3S	3S	3F	3F	-	-	-	-	-	-	-	-
MSS1P20	0	0	0	0	0	0	0	0	0	2SE	2S	2S	2S	2S	2F	3F	3N	3N	3N
MSS1P21	0	0	0	0	0	0	0	0	0	0	0	0	0	0	2SE	2SE	2SE	2S	2F
MSS1P22	0	0	0	0	0	0	0	0	0	0	0	0	0	0	0	0	0	0	0
MSS1P23	0	0	0	0	0	0	0	0	0	0	0	0	0	0	0	0	0	0	0
MSS1P24	0	0	0	0	0	0	0	1SE	1SE	2S	2F	2F	3F	3F	3F	-	-	-	-
MSS1P25	0	0	0	0	0	1SE	1SE	2SE	2SE	3S	3S	3S	3S	3S	3S	3F	3F	3F	3N
MSS1P26	0	0	0	0	0	0	0	0	0	2SE	2SE	2SE	2SE	2SE	2SE	2SE	2SE	2SE	3F
MSS1P27	0	0	0	0	0	0	0	1SE	1SE	2S	2S	3S	3F	3F	3F	3N	-	-	-
MSS1P28	0	0	0	0	0	0	1SE	2SE	2SE	2SE	2SE	2SE	2S	2F	2F	3F	3F	3F	-
MSS1P29	0	0	0	0	0	0	0	0	2SE	2SE	2SE	3S	-	-	-	-	-	-	-
MSS1P30	0	0	0	0	0	0	0	1SE	2SE	2SE	2SE	2SE	2FE	3FE	3FE	3FE	3NE	-	-

Table 36: binding energies for C1s XPS-spectrum; 0 s sputtering[58]

	BE in eV	FWHM in eV
blank	285.07	-
charging	284.01	1.79
C-O/C-Cl	286.61	1.39
C=O	288.30	1.38

Table 37: binding energies for C1s XPS-spectrum; 180 s sputtering[58]

	BE in eV	FWHM in eV
blank	284.58	-
C-C/C-H	285.44	1.00
C-O/C-Cl	286.56	1.42
O-C=O	290.03	0.75
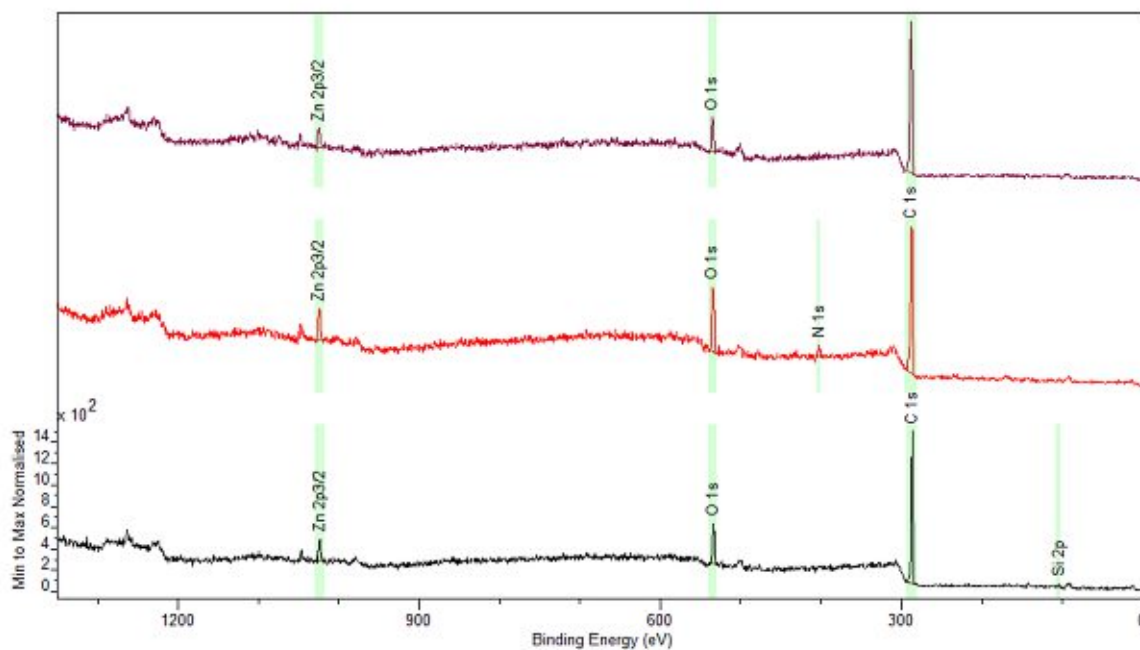
Figure 27: XPS survey spectra normalized to their strongest signal; from top to bottom: 8- and 24-hours reaction time with 200 pphm ozone and 55 % RH; undermost trace depicting the blank measurement of the unmodified test specimen; green areas were used for quantification[58]
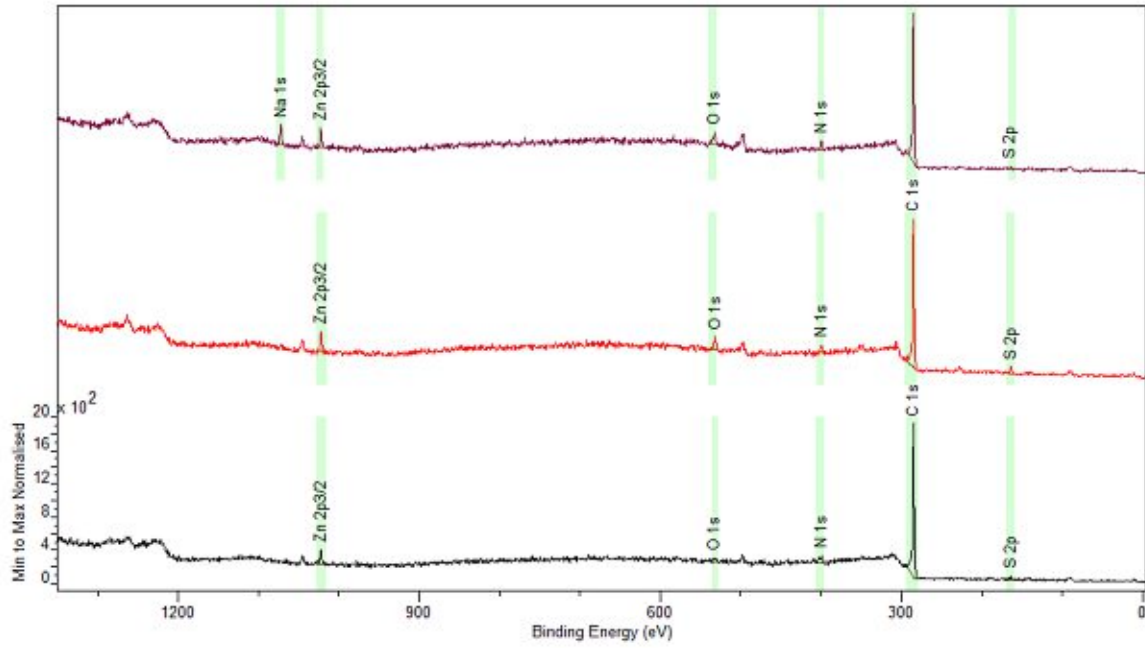
Figure 28: XPS survey spectra normalized to their strongest signal after 180 s Ar-ion sputtering; from top to bottom: 8- and 24-hours reaction time with 200 pphm ozone and 55 % RH; undermost trace depicting the blank measurement of the unmodified test specimen; green areas were used for quantification[58]
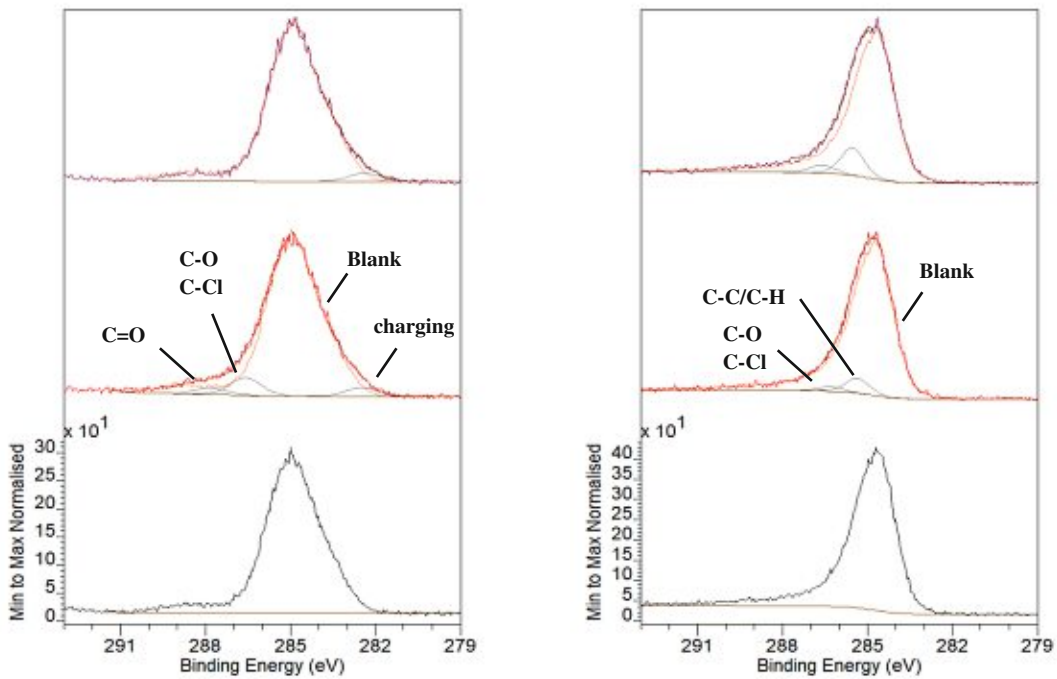

Figure 29: C1s XPS detail spectra normalized to their strongest signal after left) 0 s- and right) 180 s-Ar-ion sputtering; from top to bottom: 8- and 24-hours reaction time with 200 pphm ozone and 55 % RH; undermost trace depicting the blank measurement of the unmodified test specimen[58]
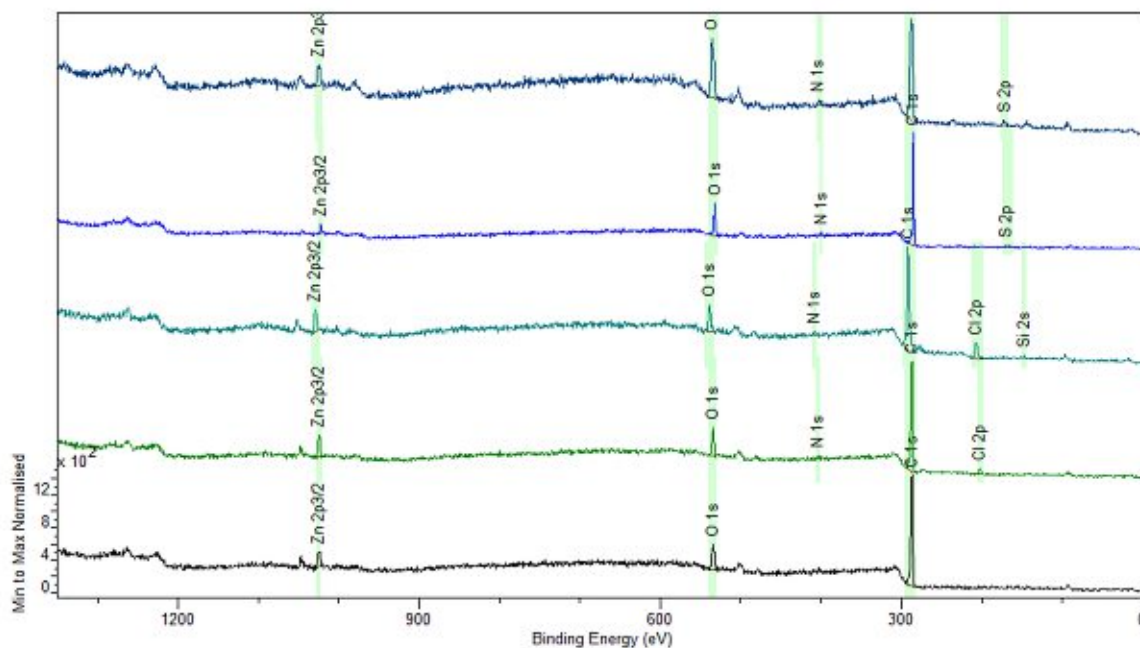
Figure 30: XPS survey spectra normalized to their strongest signal; from top to bottom: 10- and 1-min epoxidation time (30 % m-CPBA in 2-propanole), 10- and 1-min chlorination time (acidified aqueous NaOCl solution (13 %)); undermost trace depicting the blank measurement of the unmodified test specimen; green areas were used for quantification[58]
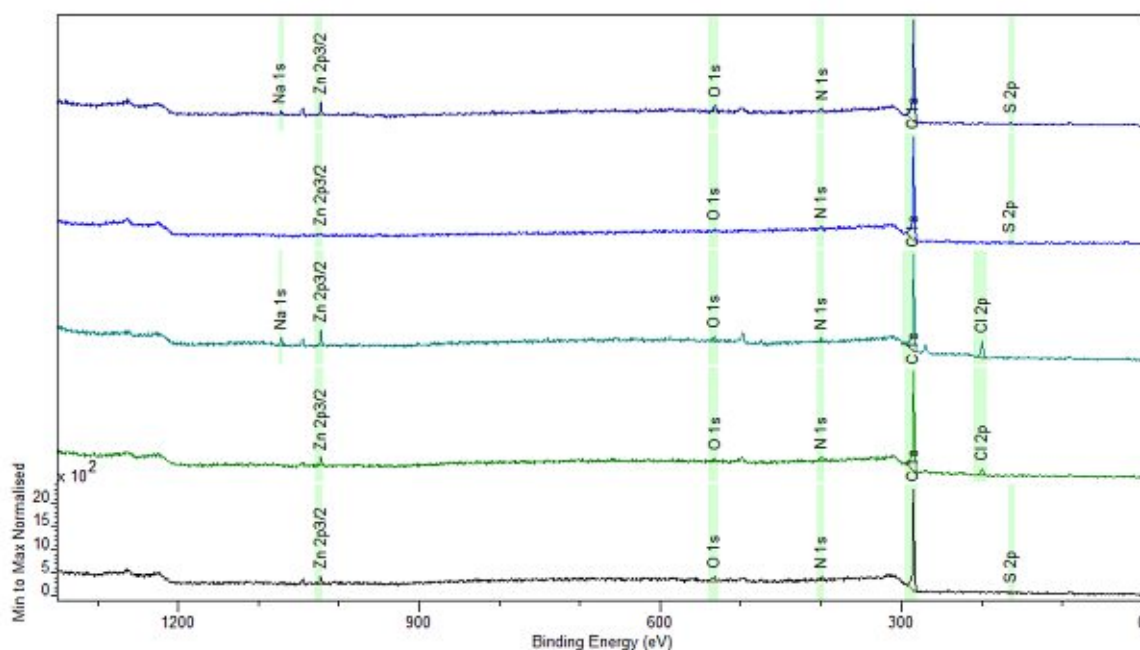

Figure 31: XPS survey spectra normalized to their strongest signal after 180 s Ar-ion sputtering; from top to bottom: 10- and 1-min epoxidation time (30 % m-CPBA in 2-propanole), 10- and 1-min chlorination time (acidified aqueous NaOCl solution (13 %)); undermost trace depicting the blank measurement of the unmodified test specimen; green areas were used for quantification[58]
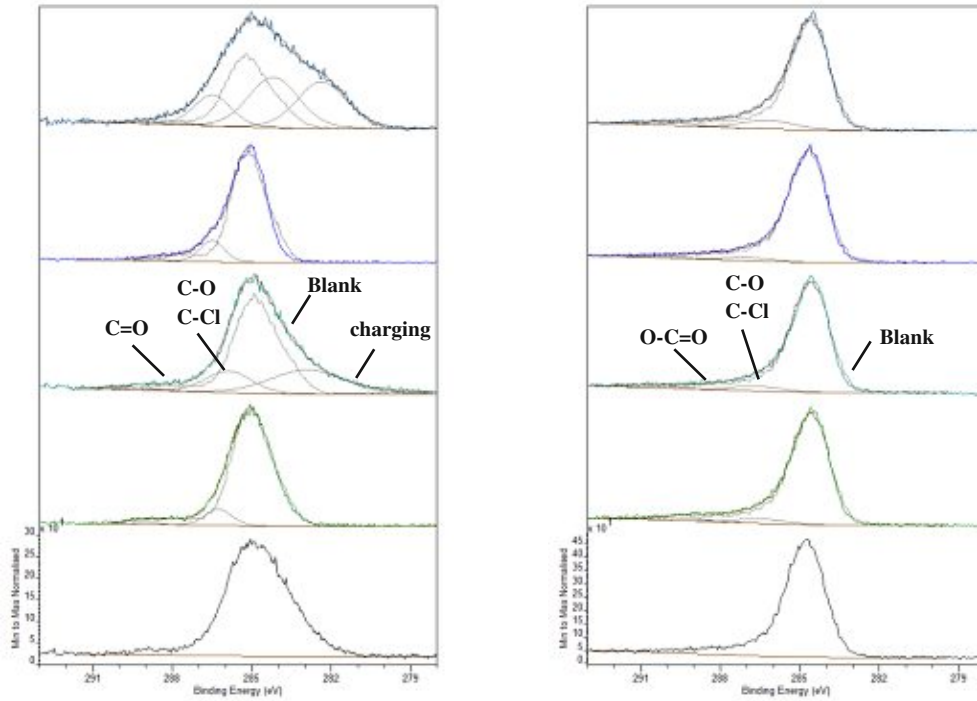
Figure 32: C1s XPS detail spectra normalized to their strongest signal after left) 0 s- and right) 180 s-Ar-ion sputtering; from top to bottom: 10- and 1-min epoxidation time (30 % m-CPBA in 2-propanole), 10- and 1-min chlorination time (acidified aqueous NaOCl solution (13 %)); undermost trace depicting the blank measurement of the unmodified test specimen[58]